Project No. 23440-909291

Microstructure of Air and Water Cured Silica Fume Concretes

by

Shondeep L. Sarkar

and

Xu Aimin*

Faculté des sciences appliquées
Université de Sherbrooke
Sherbrooke (Québec) J1K 2R1 CANADA

Reported submitted to Dr. V. Mohan Malhotra
Mineral Sciences Laboratory
CANMET, Ottawa

* Permanent address:
Division of Building Materials
Chalmers University of Technology
Göteborg, Sweden

March 1991

Project No. 23440-909291

CONTRACT SERIAL NO. 99291-01-SS
CONTRACT REQUISITION NO. 9-9291
CONTRACTOR: UNIVERSITÉ DE SHERBROOKE

Microstructure of Air and Water Cured Silica Fume Concretes

by

Shondeep L. Sarkar

and

Xu Aimin*

Faculté des sciences appliquées
Université de Sherbrooke
Sherbrooke (Québec) J1K 2R1 CANADA

Reported submitted to Dr. V. Mohan Malhotra
Mineral Sciences Laboratory
CANMET, Ottawa

* Permanent address:
Division of Building Materials
Chalmers University of Technology
Göteborg, Sweden

March 1991

82 pp

MICROMEDIA

INTRODUCTION

As a part of the on-going project (of the Mineral Sciences Laboratory, CANMET) on the long-term durability of silica fume (SF) concrete, the microstructure of 12 concretes at age 3 1/2 years were investigated by the writers.

The mixing schedule and curing regime of these concretes are shown in Table 1, and the mix proportions and properties of fresh concretes in Table 2.

From Table 1 it is clear that the W/C+SF ranges from 0.25 to 0.40. Furthermore, for each W/C+SF ratio (0.25, 0.30, 0.40) batch of concrete cured under two different curing regimes, two sets of concretes were made without any silica fume at the same W/C ratio. These are labelled "control" or reference concretes (G1, G2, G5, G6, G9 and G10) in Tables 1 and 2.

The slump loss for these concretes varies between 100 and 200 mm (Table 2). The air content lies between 1.6 and 2.3% from G1 to G3 concrete, but in G4 to G12 it is around 6.5%. The unit weight was maintained between 2330 and 2520 kg/m^3. The total cementitious content decreases steadily from 540 to 350 kg/m^3 from the 0.25 W/C+SF batch to the 0.40 batch. A fixed amount of SF (10% by mass) was used in all the six SF concretes (G3, G4, G7, G8, G11 and G12).

OBJECTIVE

The primary objective of this study was to determine from microstructural investigation whether any differences exist between the air and the water cured SF concretes that can influence their engineering properties and later-age performance.

It must be pointed out that to the best of writers' knowledge, no microstructural investigation of this nature has previously been cited in the literature.

Table 1
Mixing Schedule and Curing Regime

Mix No.	Date of Mixing	W/(C+SF)	Type of Concrete	Curing Regime
G1	July 30/87	0.25	Control	Water*
G2	Aug. 4/87		Control	Air**
G3	Aug. 6/87		10% SF	Water
G4	Aug. 11/87		10% SF	Air
G5	Aug. 18/87	0.30	Control	Water
G6	Aug. 20/87		Control	Air
G7	Aug. 27/87		10% SF	Water
G8	Sept. 1/87		10% SF	Air
G9	Sept. 3/87	0.40	Control	Water
G10	Sept. 8/87		Control	Air
G11	Sept. 10/87		10% SF	Water
G12	Sept. 15/87		10% SF	Air

* Continuously water-cured (at room temperature)
** Continuously air-cured (at ambient room conditions) after initial water-curing for 7 days

Table 2
Mix Proportions and Properties of Fresh Concrete

Mix No.	Silica Fume, %	W/(C+SF)	Total cementitious, kg/m^3	Coarse/Fine Agg.	Slump, mm	Unit Weight, kg/m^3	Air, %
G1	0	0.25	540	62/38	175	2500	2.3
G2	0	0.25	540	62/38	175	2520	2.1
G3	10	0.25	540	62/38	200	2520	1.6
G4	10	0.25	540	62/38	175	2520	1.7
G5	0	0.30	460	62/38	150	2350	6.5
G6	0	0.30	460	62/38	125	2370	6.2
G7	10	0.30	460	62/38	125	2330	6.6
G8	10	0.30	460	62/38	150	2350	6.4
G9	0	0.40	350	60/40	100	2330	6.8
G10	0	0.40	350	60/40	125	2350	6.5
G11	10	0.40	350	60/40	150	2330	6.2
G12	10	0.40	350	60/40	150	2330	6.4

Notes: (1) Max size of agg.: 12 mm for mixes G1 to G4 and 19 mm for mixes G5 to G12
(2) Naphthalene-based superplasticizer used in all mixes

METHODS

A JEOL JSM-840A SEM/Link 100085 EDXA was used to study the general microstructural features. A Rigaku D-Max XRD was used to determine semiquantitatively the amount of CH in each concrete, by peak integration (PI) (Fig. 1) and peak height measurement. The PI method consists of calculating the integrated intensity of the 001 peak of CH at 18.04°2θ. The selection of the total area under the peak is arbitrary, and can vary from one operator to the other. In this case the peak area selected ranged from 17.40° to 18.24°2θ. However, anomalies can arise due to preferred orientation of the basal (001) reflection at 18.04°2θ. Hence, another strong peak of CH at 34.08°2θ was also selected. Since peak overlap with feldspar in this region is unavoidable, only the peak height was measured in this case.

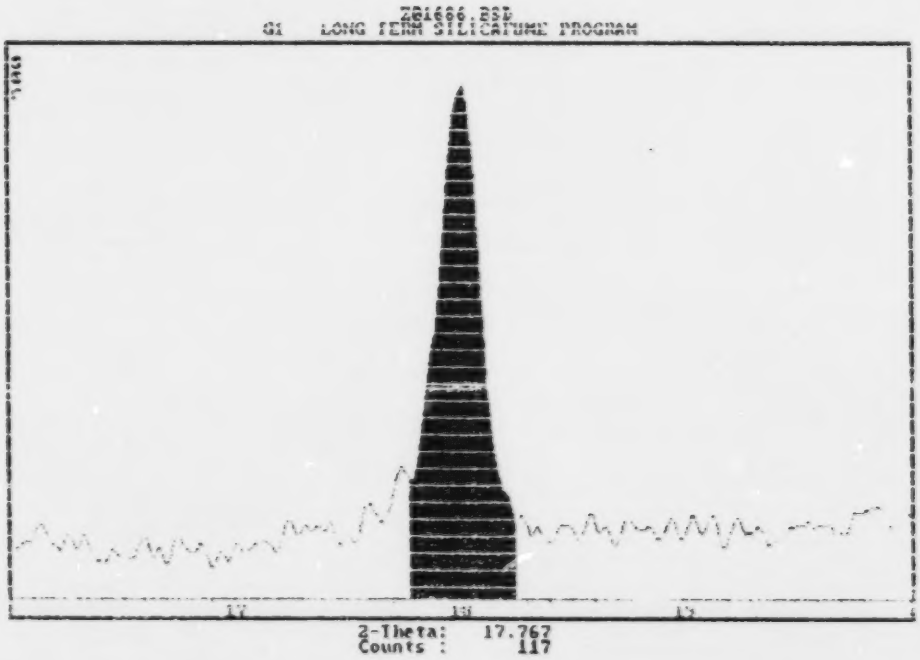

Fig. 1 An example of the peak area selected (shaded) for peak integration of the 001 peak of CH at 18.04°2θ

A very similar peak integration procedure was adopted for Ca/Si ratio determination of C-S-H when analyzing the concretes by EDXA (Fig. 2).

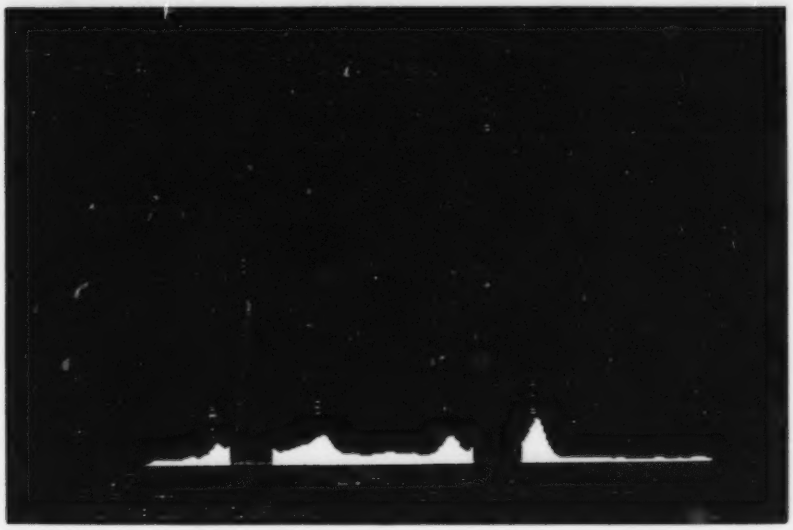

Fig. 2 A typical EDXA spectrum of C-S-H. Ca and Si peaks shaded grey indicate that windows were inserted on these two elemental peaks to obtain the integral value of these peaks

RESULTS

(i) SEM/EDXA

G3 concrete, with 10% SF, water cured, W/C+SF = 0.25

The microstructure of this concrete comprises dense paste (Fig. 3) with very fine micropores (< 1 μm).

Some short microfissures (< 1 μm in width) are present (Fig. 4). A number of these seem to originate at the periphery of unhydrated cement grains, and travel to pores, where they appear to be arrested (Fig. 5).

A large number of unhydrated and slightly hydrated cement grains are present (Figs. 5 and 6).

A few small irregular grains of CH were observed in the paste (Figs. 7 and 8).

G3 Concrete

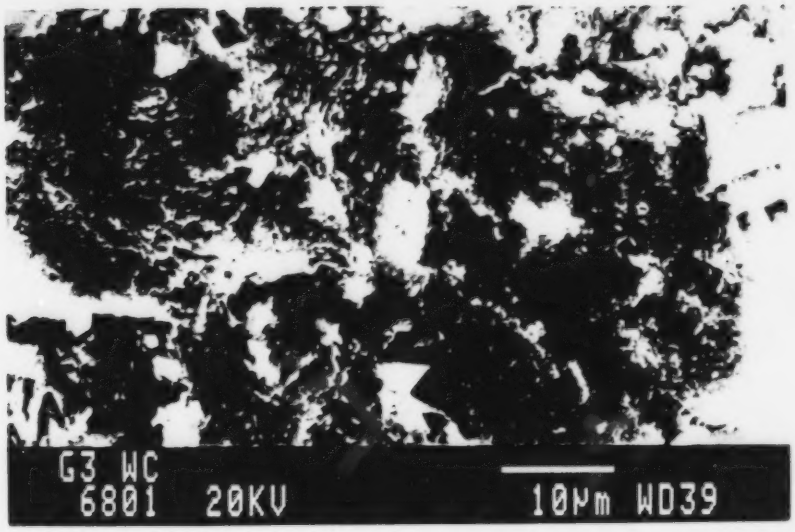

Fig. 3 Dense paste. A few Micropores are visible

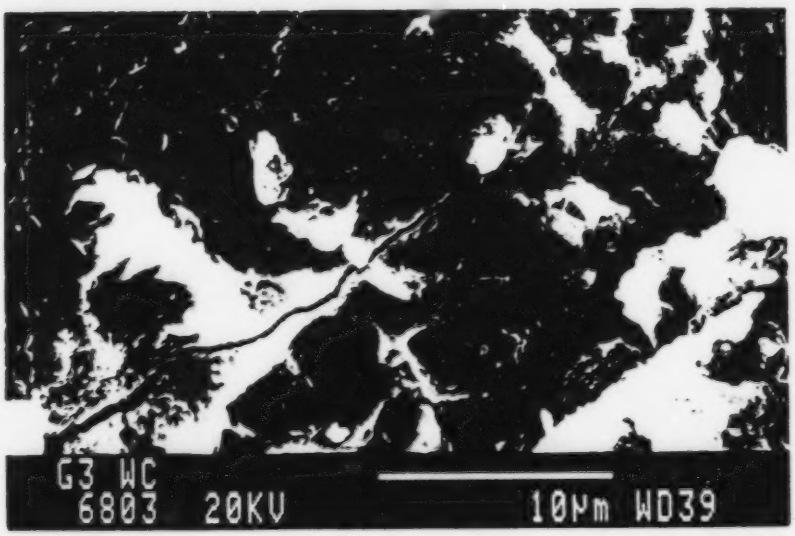

Fig. 4 A microfissure (< 1 µm in width) in the paste

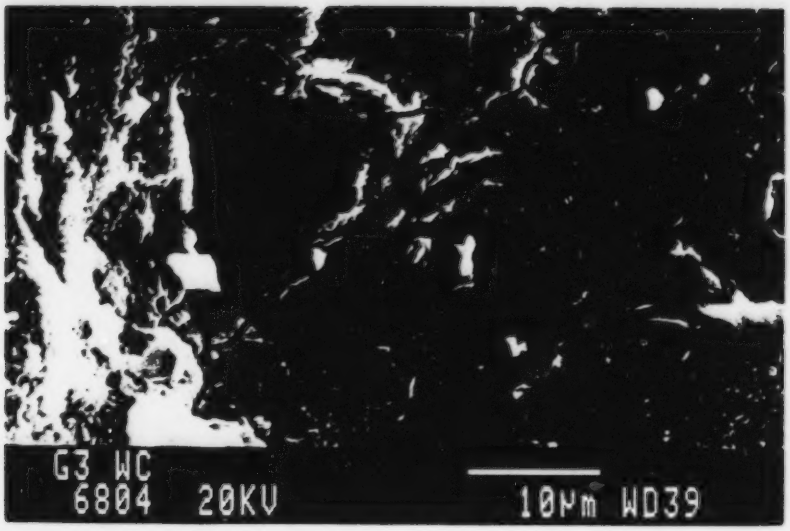

Fig. 5 A microfissure around an unhydrated cement grain seen to travel up to a pore

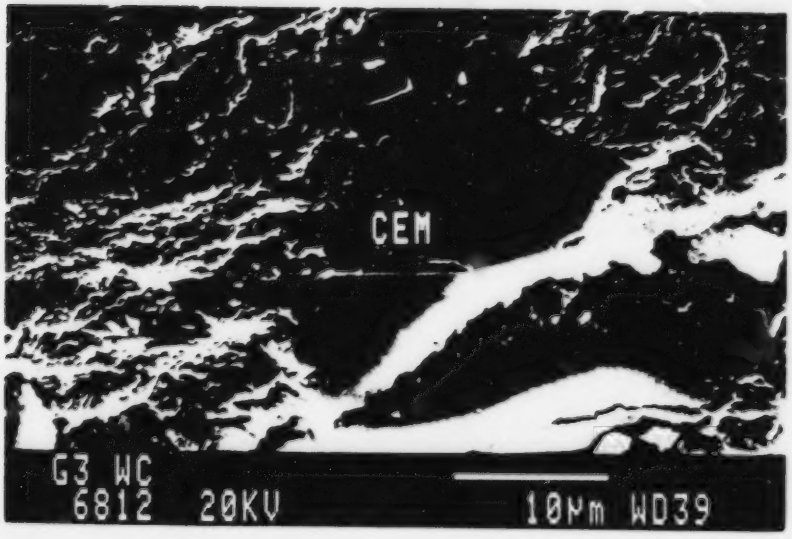

Fig. 6 A partly hydrated cement grain in the paste

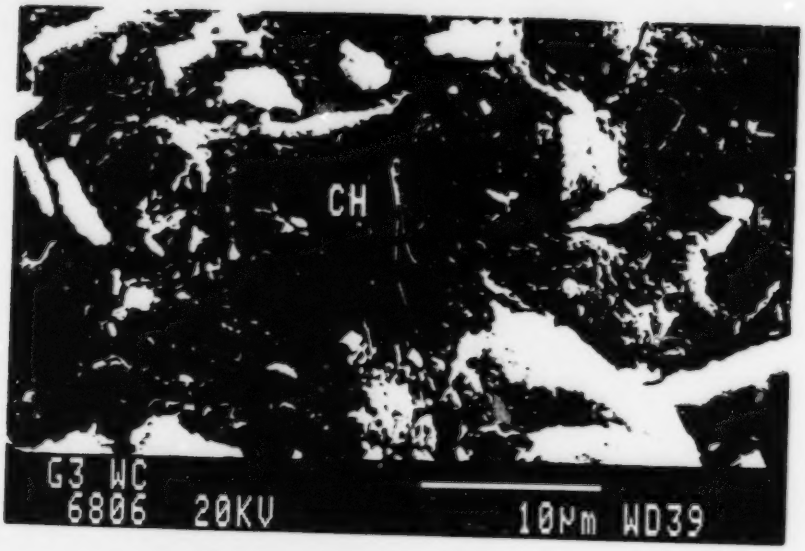

Fig. 7 Small irregular CH in the paste

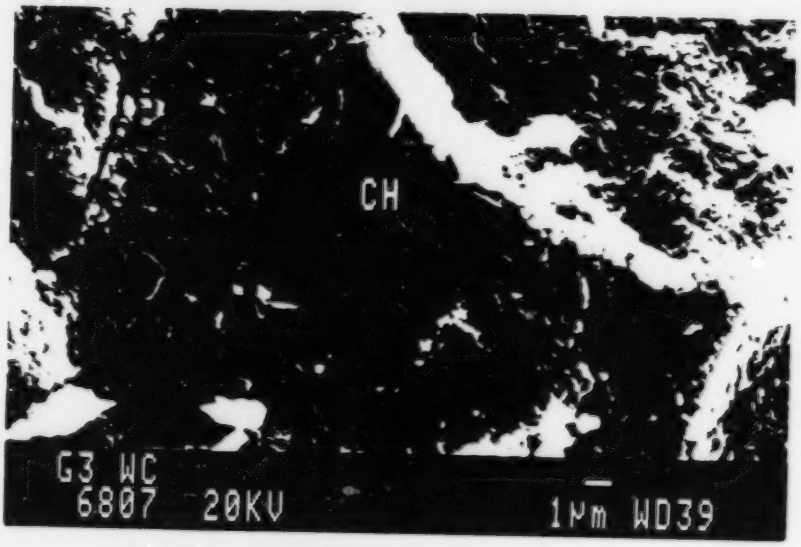

Fig. 8 Same

The paste-aggregate bonding is very strong (Figs. 9 and 10). The transition zone* is composed mainly of C-S-H (Fig. 11), but is slightly more porous than the matrix. Some stacked type of CH with irregular morphology can be seen in this region.

No ettringite was visible either in the paste or in the transition zone. The absence of ettringite was confirmed from XRDA. The low quantity of CH was also evident from XRDA (discussed in a later section).

---

* The transition zone was examined after carefully fracturing the specimen along this zone.

Fig. 9 Strong paste-aggregate bonding

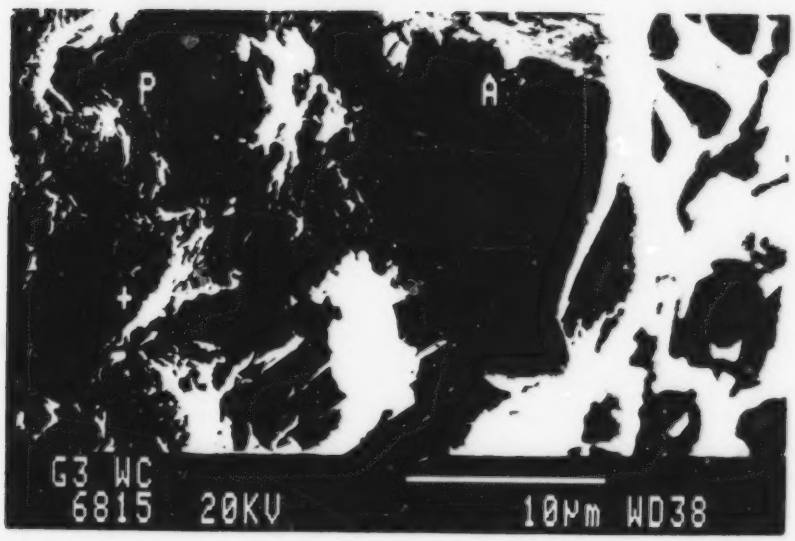

Fig. 10 Same

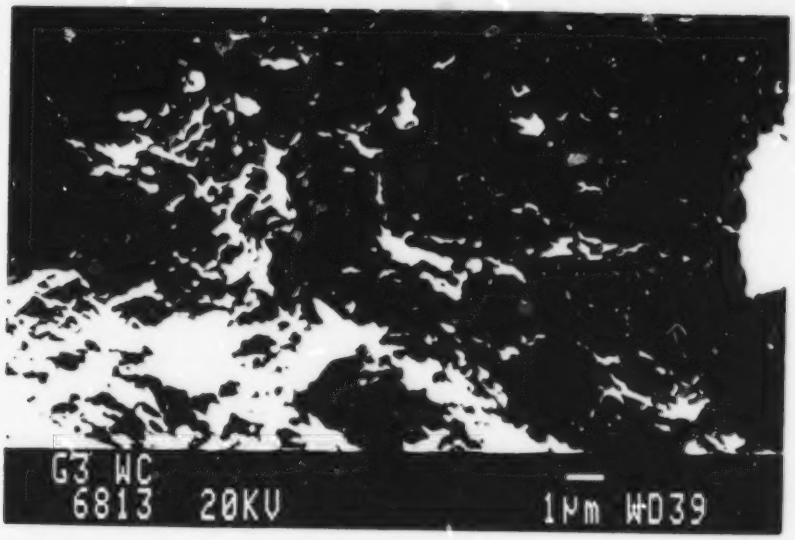

Fig. 11 Transition zone composed of C-S-H. Increased porosity is evident

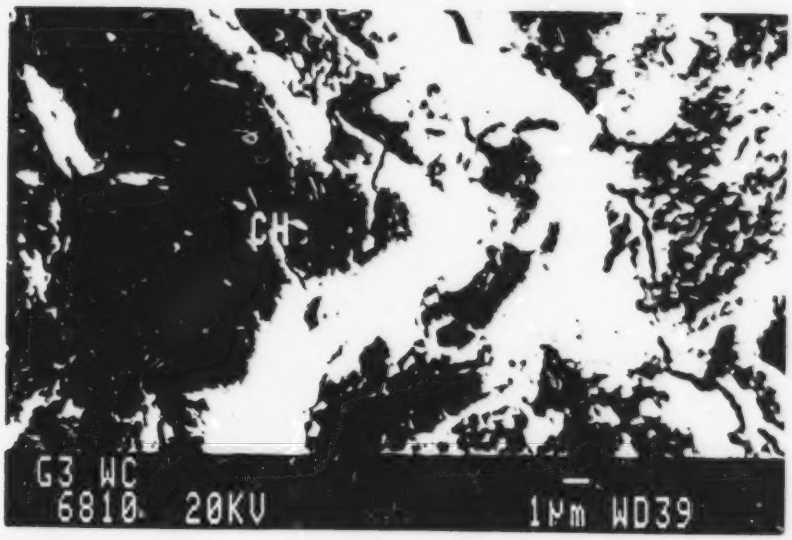

Fig. 12 Stacked CH crystals with irregular morphology in the transition zone

Fig. 9 Strong paste-aggregate bonding

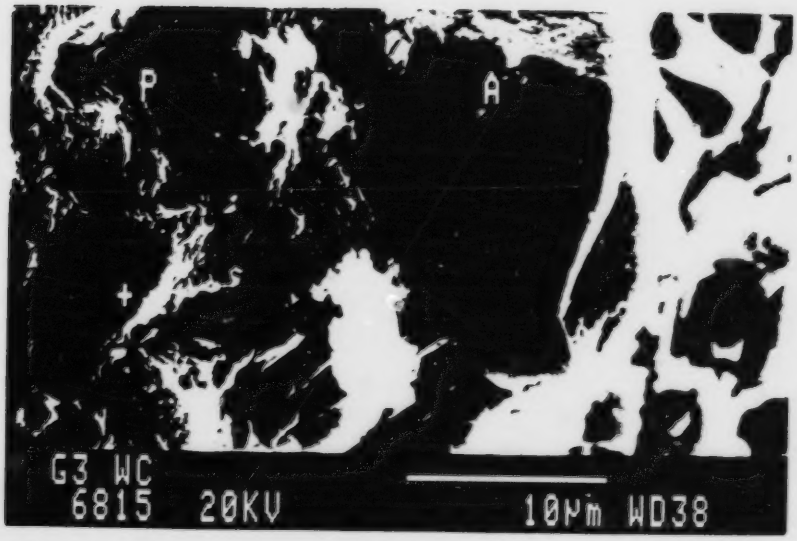

Fig. 10 Same

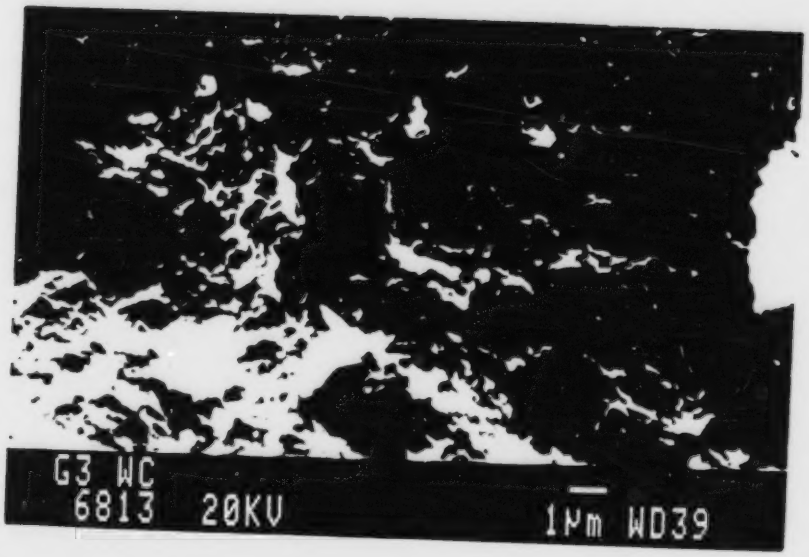

Fig. 11 Transition zone composed of C-S-H. Increased porosity is evident

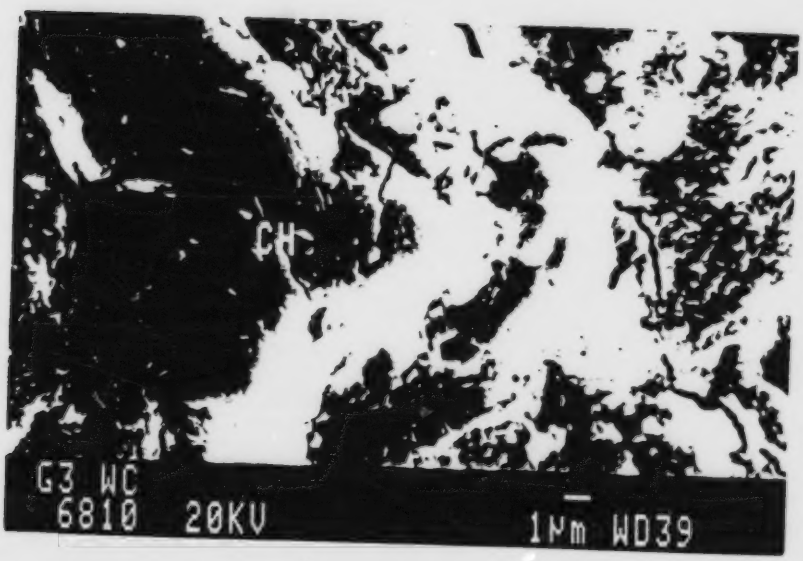

Fig. 12 Stacked CH crystals with irregular morphology in the transition zone

G1 control concrete, without SF, water cured, W/C = 0.25

Reaction rim of cement grains are vivid in this concrete (Fig. 13). Similar to its counterpart concrete (G3), it contains several unhydrated and partly hydrated cement grains (Fig s 13 and 14). The paste is not uniformly dense as in G3 concrete (Figs. 15 and 16). Both large irregular and well-crystallized CH are present (Figs. 17 and 18). In some localities perfect hexagonal plates of CH (Fig. 19) and ettringite needles were observed (Fig. 20).

The paste-aggregate bond varies from porous (Fig. 21) to strong (Fig. 22). Some parts of the transition zone contain abundant hexagonal CH plates (Fig. 23), whereas other parts comprise only C-S-H (Fig. 24). The part with CH crystals in it most likely represents the bottom of the aggregate where is higher accumulation of water resulted in elevated quantity of CH formation. As in G3 concrete, the transition zone exhibits higher porosity.

G1 Concrete

Fig. 13 Reaction rim around a cement grain

Fig. 14 A partly hydrated cement grain in the paste

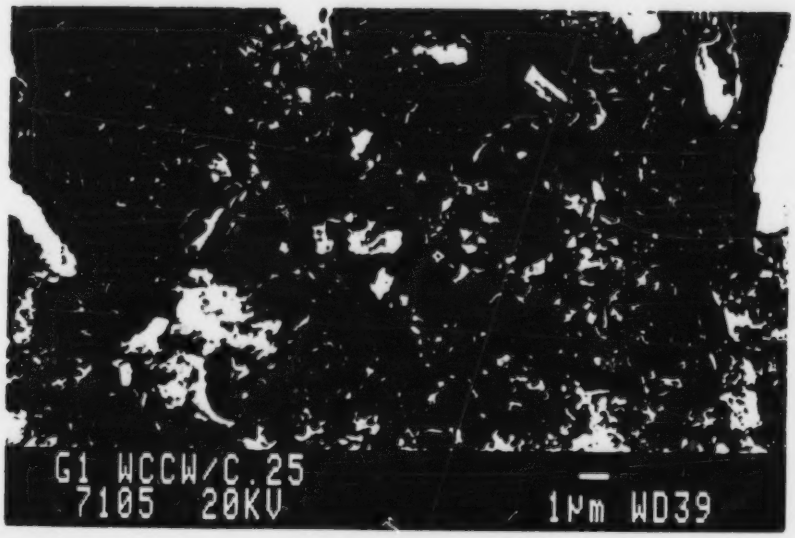

Fig. 15 Dense part of the paste

Fig. 16 Another part of the paste that is porous

Fig. 17 Large but irregular CH

Fig. 18 Much more well crystallized CH

Fig. 19 Hexagonal CH plates

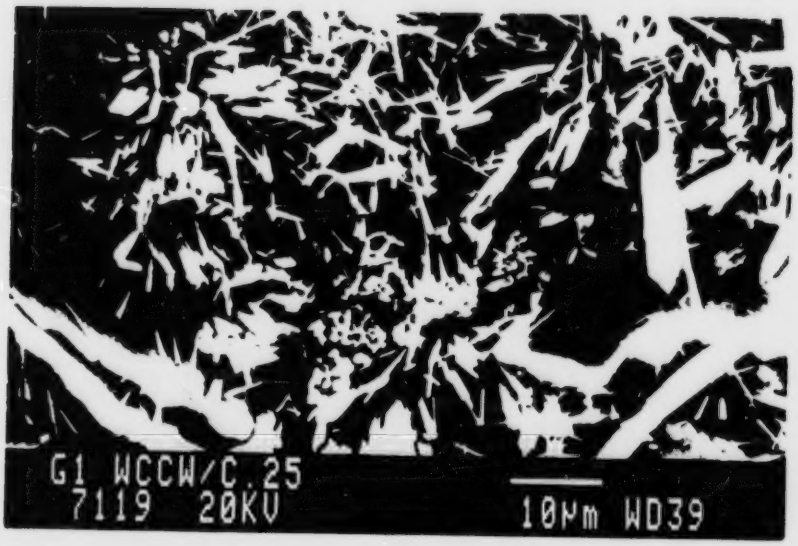

Fig. 20 Ettringite needles in the paste, associated with platy CH crystals

Fig. 21 Porous paste-aggregate interface

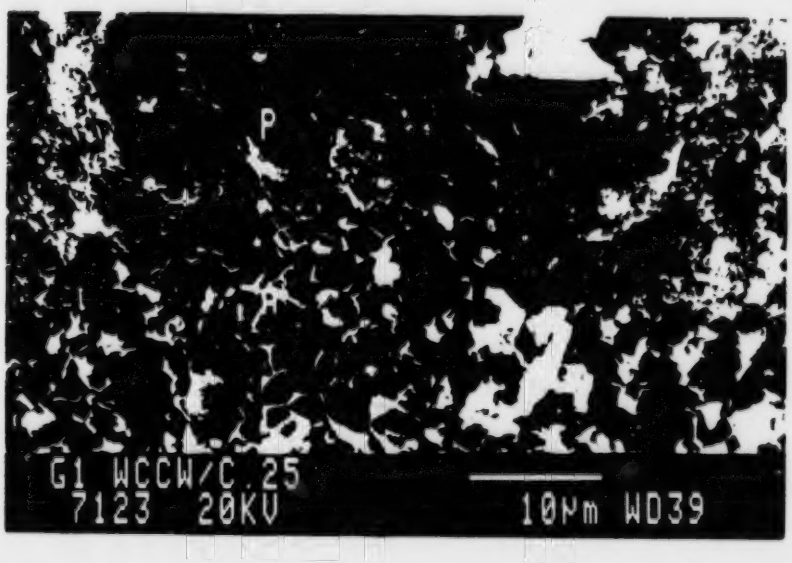

Fig. 22 Strong paste-aggregate interface

Fig. 23 CH plates in the transition zone

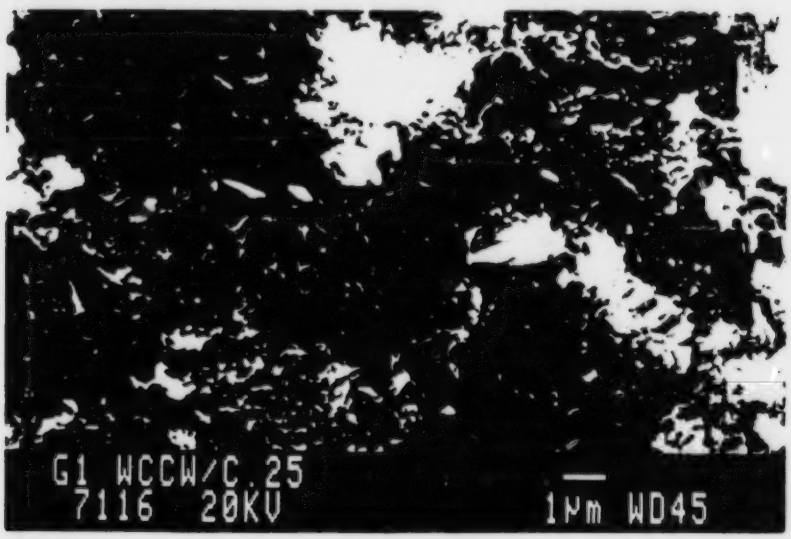

Fig. 24 C-S-H in the transition zone. Increased porosity can be seen

G2 control concrete, without SF, air cured, W/C = 0.25

The morphology of C-S-H appears to be different, in the sense it shows short fibrous features (Fig. 25). This type of CH has been classified as type I C-S-H by Diamond (1). The paste, unlike G3 concrete is less dense, as can be seen in Figures 25 and 26. CH, though not very regular geometrically, is large in size (Fig. 26). Unhydrated cement grains are present in this concrete also (Fig. 27). The paste-aggregate bond in some places consists of C-S-H (Fig. 28), whereas in others comprises massive CH (Fig. 29).

No ettringite or the hexagonal platy type of CH seen in G1 water cured control concrete was observed in this control specimen.

The transition also exhibits very similar microstructure as the paste. Irregular CH crystals (Fig. 30), partly hydrated cement grains (Fig. 31) and C-S-H with fibrous outgrowths (Fig. 32) are present in this zone.

No distinct difference in porosity between the paste and the transition zone was observed.

G2 Concrete

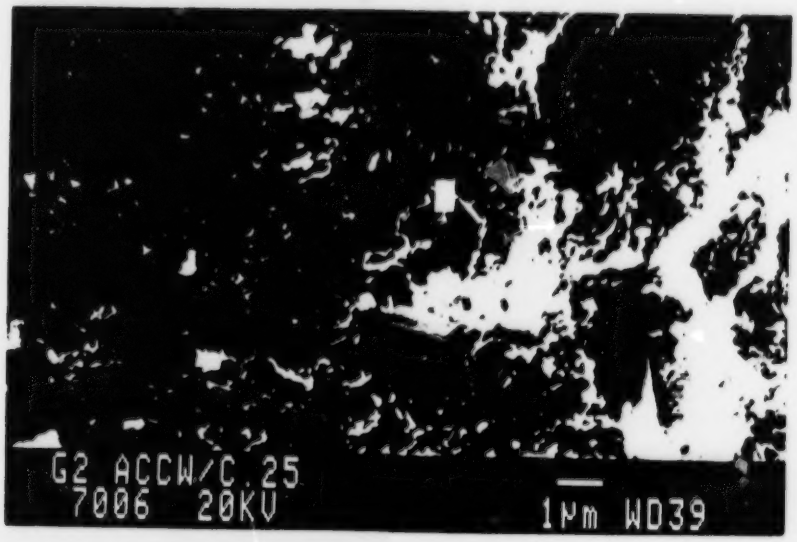

Fig. 25 C-S-H with short fibres. Somewhat porous paste

Fig. 26 A large CH crystal in the paste

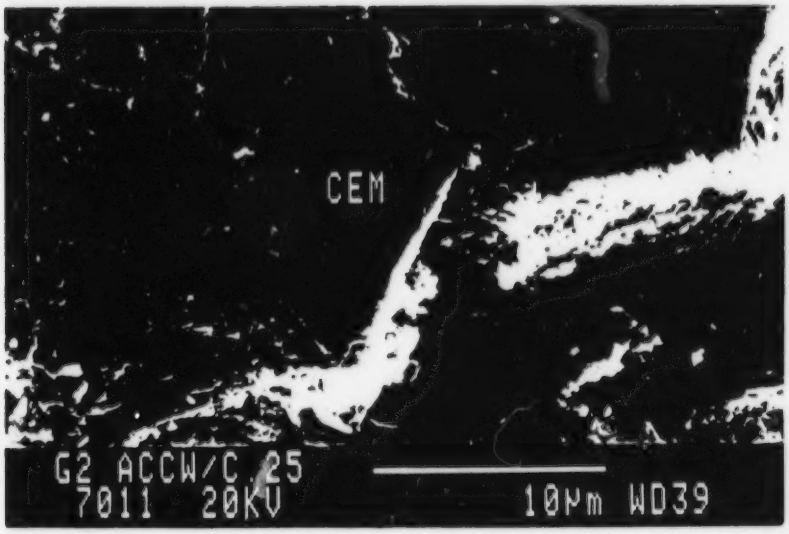

Fig. 27 An unhydrated cement particle in the paste

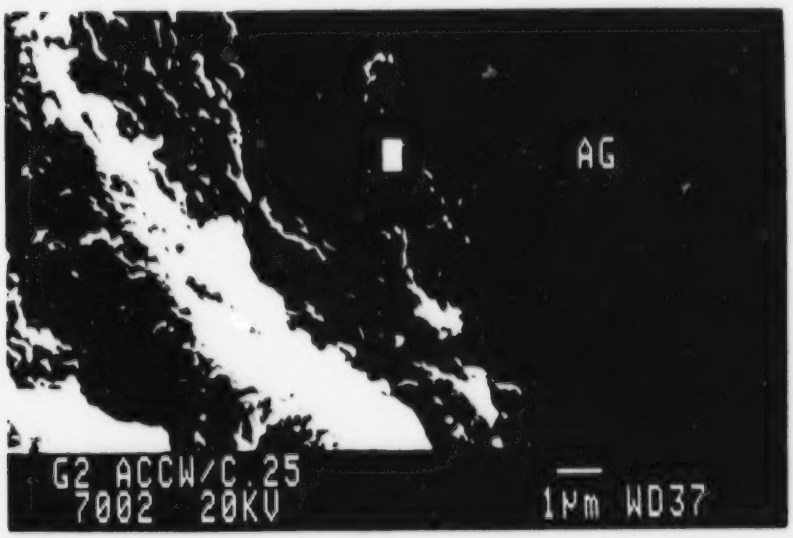

Fig. 28 Paste-aggregate interface consisting of C-S-H

Fig. 29 Paste-aggregate interface with massive CH

Fig. 30 Irregular shaped CH crystals in the transition zone

Fig. 31 Partly hydrated cement grain in the transition zone

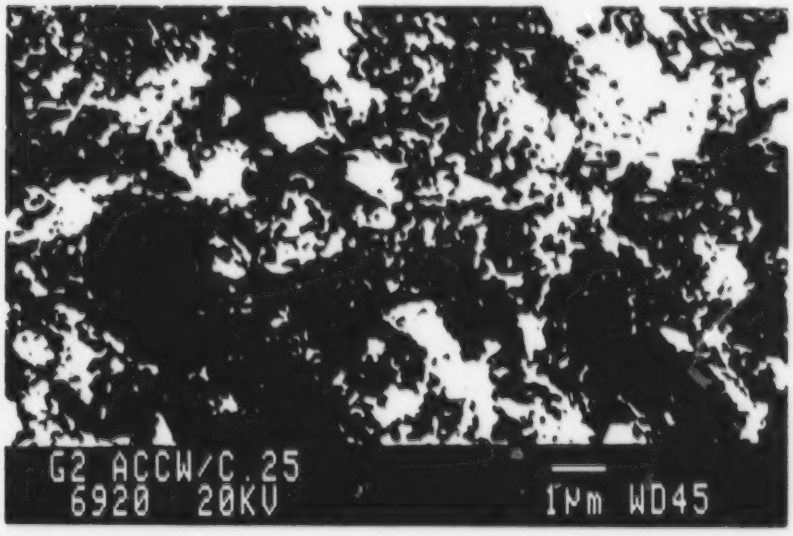

Fig. 32 C-S-H with fibrous outgrowths in the transition zone

G4 Concrete, with 10% silica fume, air cured, W/C+S F= 0.25

Unlike the G2 air cured control concrete, this concrete has a more dense paste (Fig. 33). It is very similar to its water cured counterpart concrete G3. Unhydrated cements grains are present (Fig. 34). Shrinkage cracks around cement grains are visible (Fig. 35) as in G3. The paste-aggregate bonding remains strong (Figs. 36 and 37). The transition zone is distinctly more porous than G3 concrete (Figs. 38 and 39). Some small hexagonal plates and needle structures were also visible in pores in this zone (fig. 40). Though they could not be analyzed by EDXA, they are most like CH and ettringite respectively.

G4 Concrete

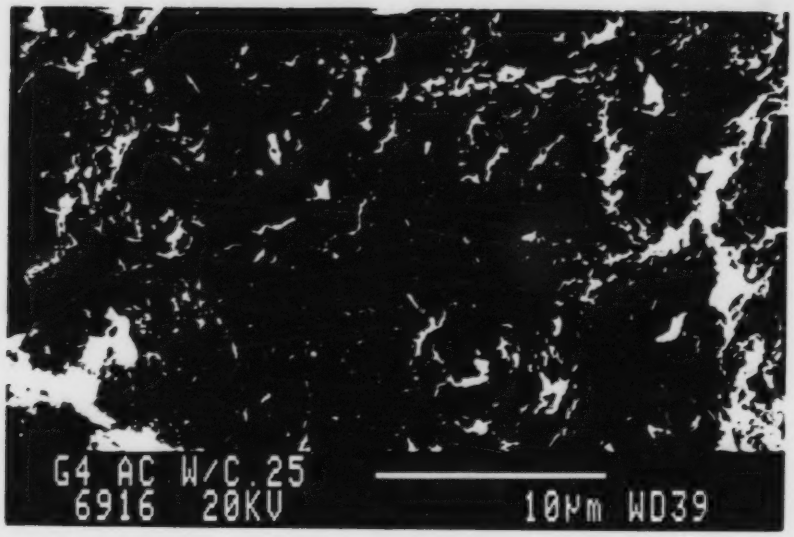

Fig. 33 Dense paste

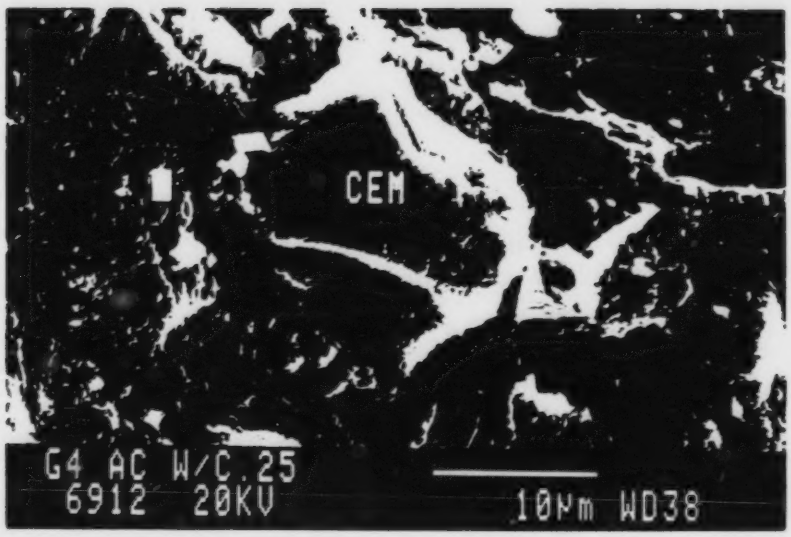

Fig. 34 Unhydrated cement grain in the paste

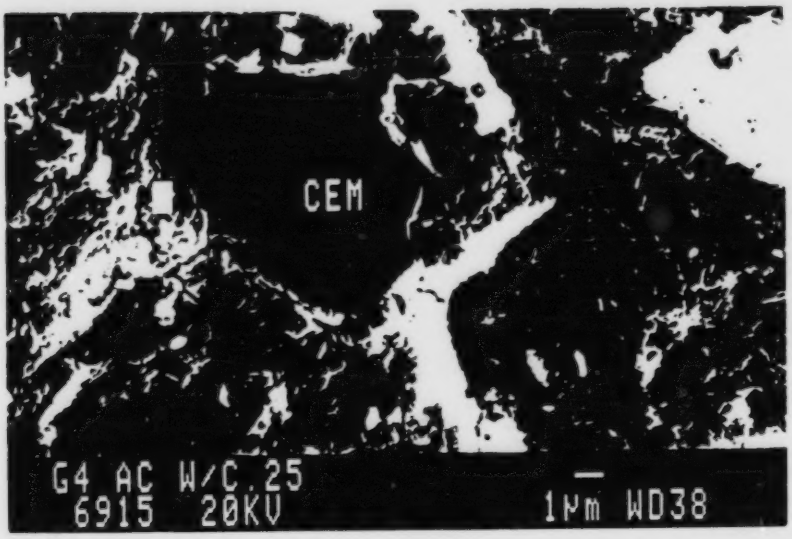

Fig. 35 A fine fissure around a cement grain

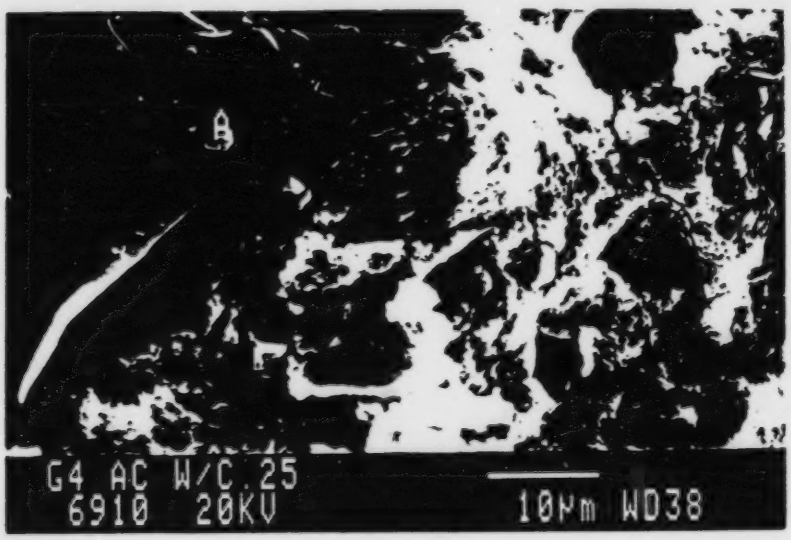

Fig. 36 Strong paste-aggregate bonding

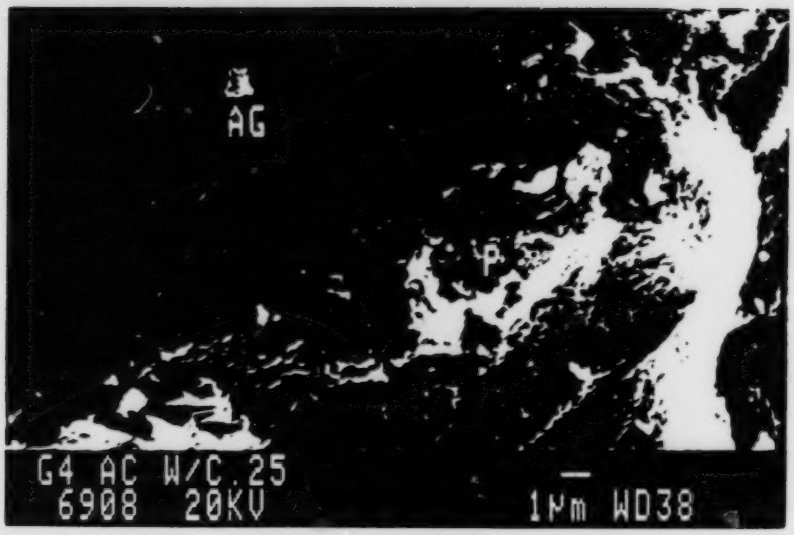

Fig. 37 Same

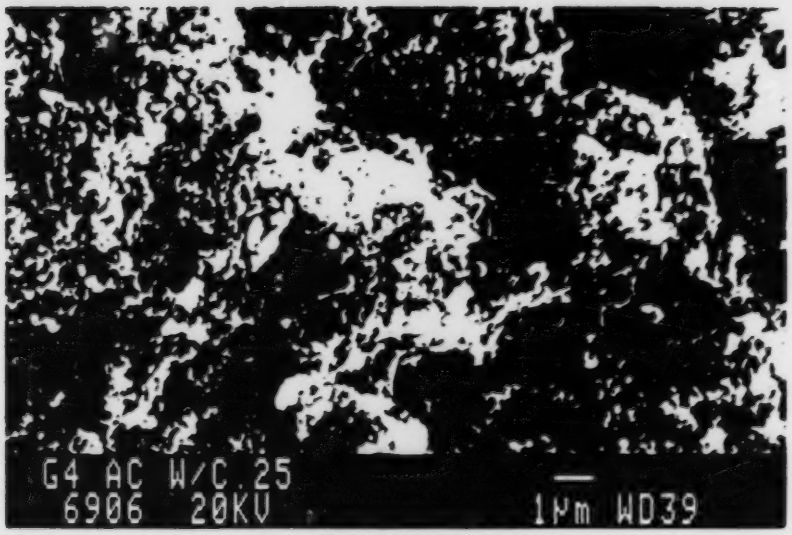

Fig. 38 Porous transition zone

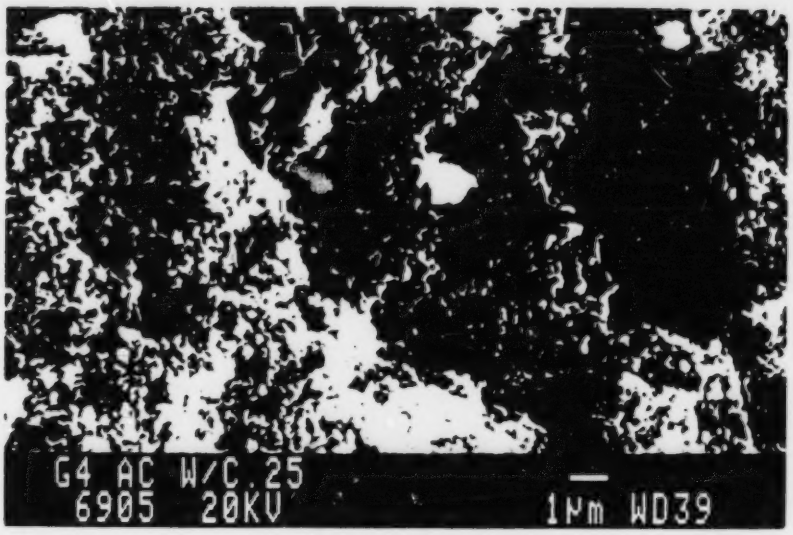

Fig. 39 Same

Fig. 40 Small hexagonal plates and needles in a pore in the transition zone

G7 Concrete, with 10% SF, water cured, W/C+S = 0.30

Despite the slight increase in W/C ratio from 0.25 to 0.30, the paste is still dense (Fig. 41). The stacking morphology of CH begins to appear (Fig. 42), but the crystals have not increased in dimension. Partly hydrated cement grains with associated CH can be seen (Fig. 43). Shrinkage cracks around cement particles are present (Fig. 44). The paste-aggregate interface comprises C-S-H in parts (fig. 45) and slightly oriented CH in other sections (Fig. 46). It is strong when C-S-H is present at the interface. The transition zone is composed mostly of C-S-H with perhaps slightly increased porosity (Fig. 47) as in G3 concrete.

G7 Concrete

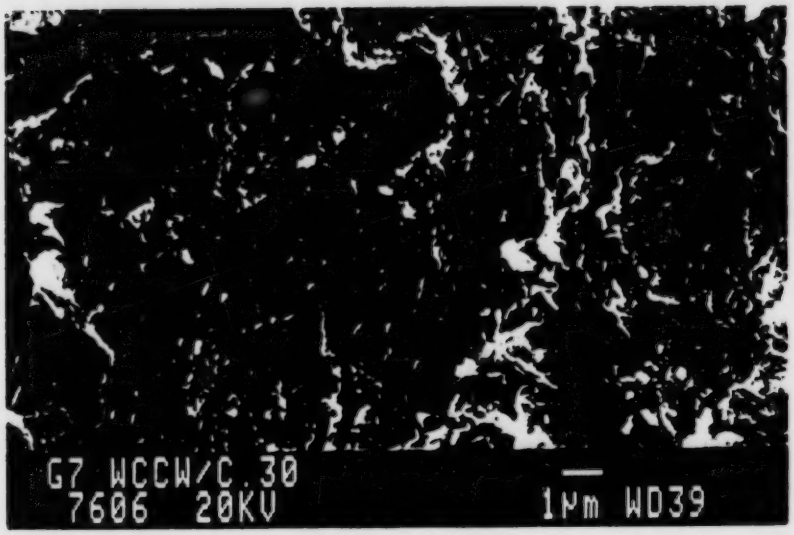

Fig. 41 Dense paste

Fig. 42 Stacking morphology of some small CH crystals

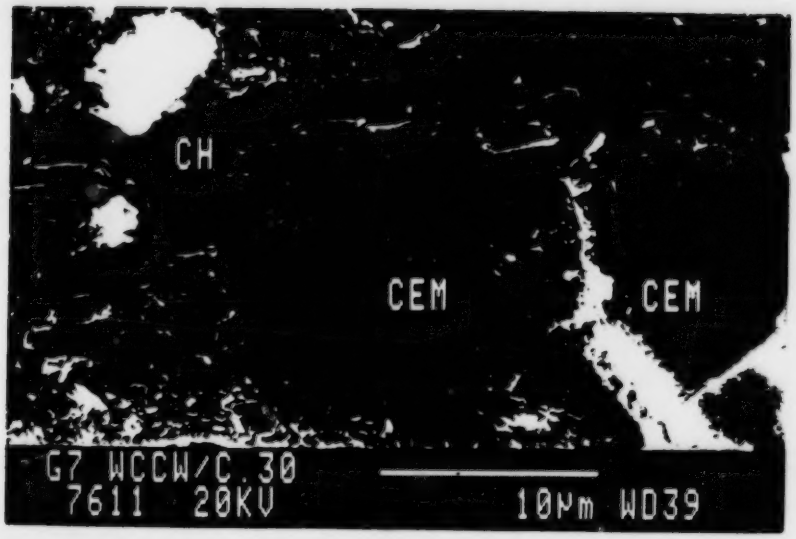

Fig. 43 Partly hydrated cement grains with CH surrounding parts of these grains

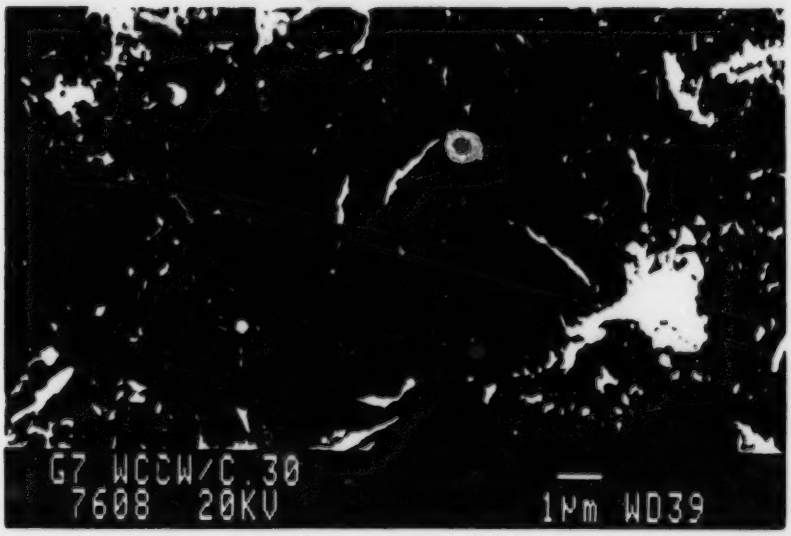

Fig. 44 Shrinkage crack around a cement grain

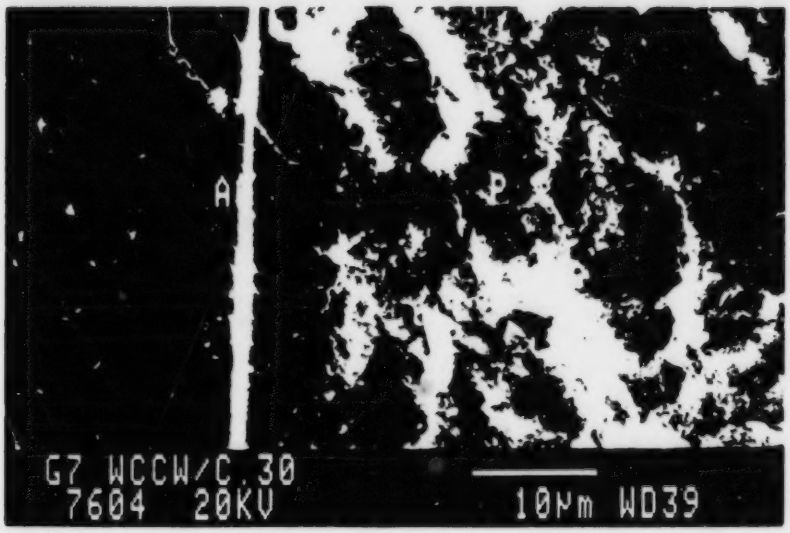

Fig. 45 Strong paste-aggregate bonding comprising C-S-H

Fig. 46 Slightly oriented CH at the interface

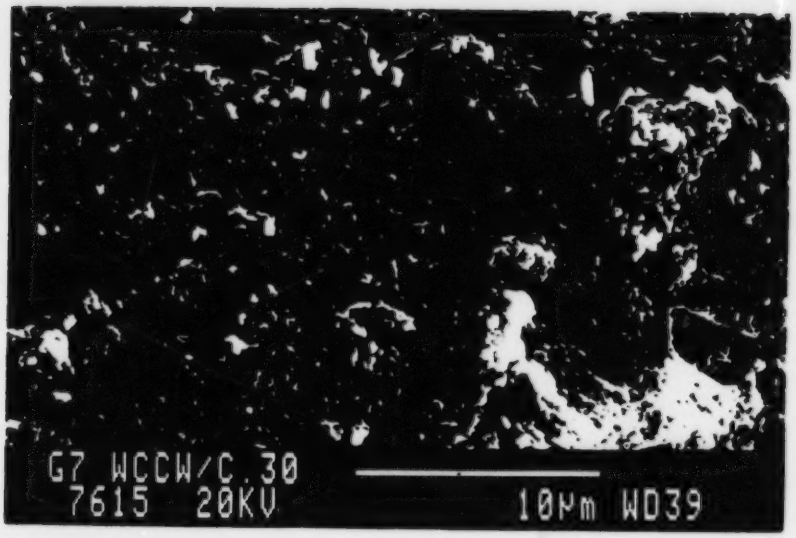

Fig. 47 Transition zone containing C-S-H

G5 control concrete, without silica fume, water cured, W/C = 0.30

This control concrete shows significant amount of large, stacked CH crystals (Figs. 48 and 49). Otherwise the paste is quite dense (Fig. 50). Distinct orientation of CH crystals is present at the paste-aggregate interface (Figs. 51 and 52). In some vacant spaces ettringite needles and hexagonal plates of CH are present (Fig. 53). Reaction rims of cement grains were also observed in (Fig. 54) as in the 0.25 W/C ratio water cured control concrete.

The transition zone is porous (Fig. 55). Considerable amount of hexagonal plates of CH and ettringite are present in this zone (Fig. 56).

As far as platy CH crystals and ettringite is concerned, this concrete closely resembles G1 control concrete, also water cured, except that stacked morphology of CH crystals were not observed in G1.

G5 Concrete

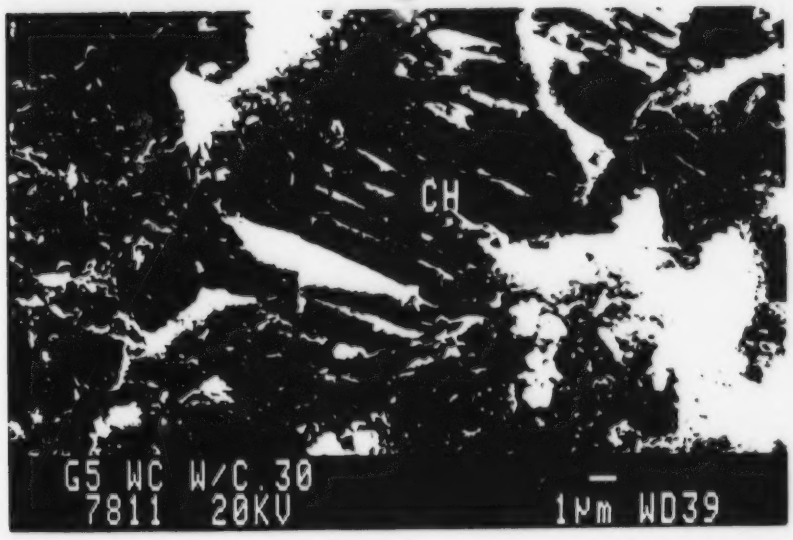

Fig. 48 Stacked CH crystals occupying over 20 μm space in the paste

Fig. 49 Large stacked CH crystals in the paste

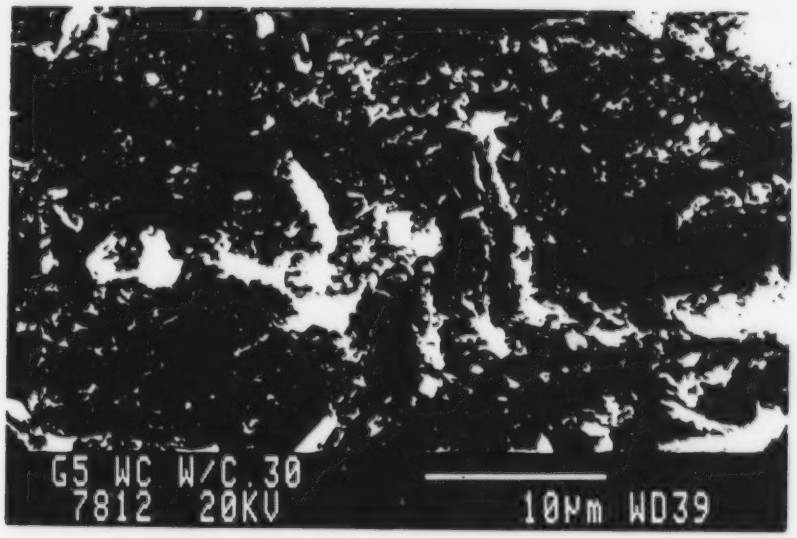

Fig. 50 Dense paste

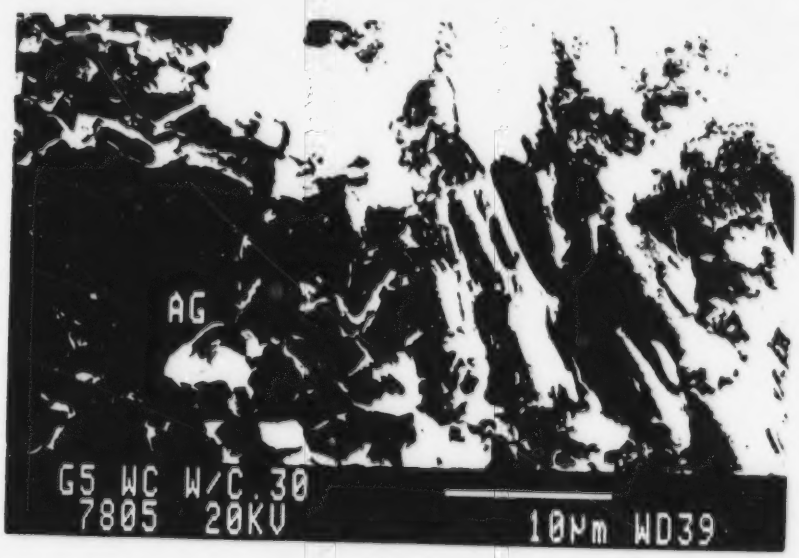

Fig. 51 Oriented CH crystals at the paste-aggregate interface

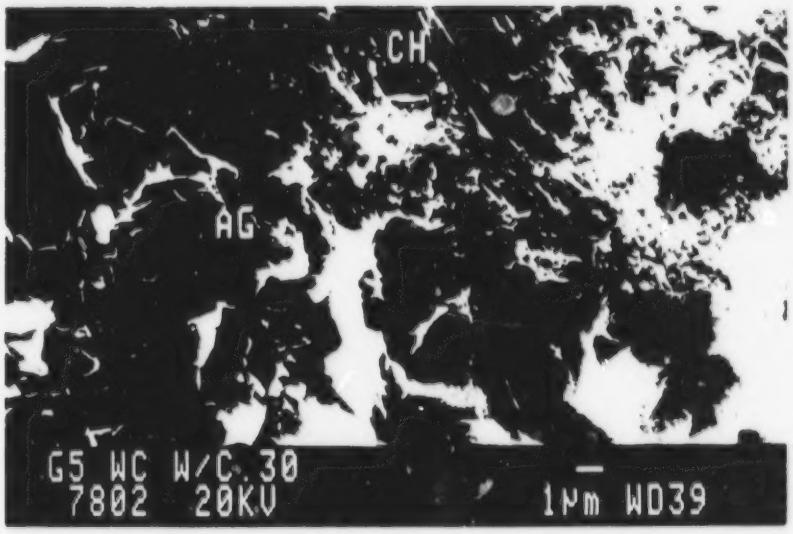

Fig. 52 Same

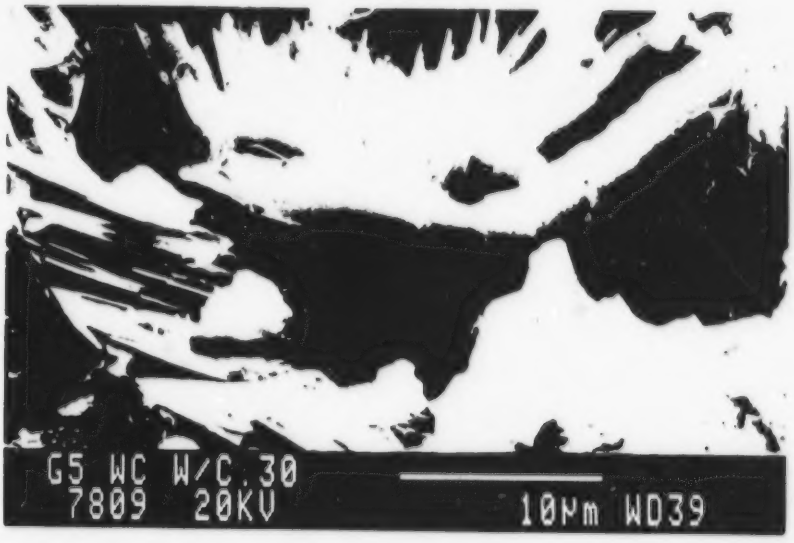

Fig. 53 Ettringite needles and platy CH crystals in a vacant space

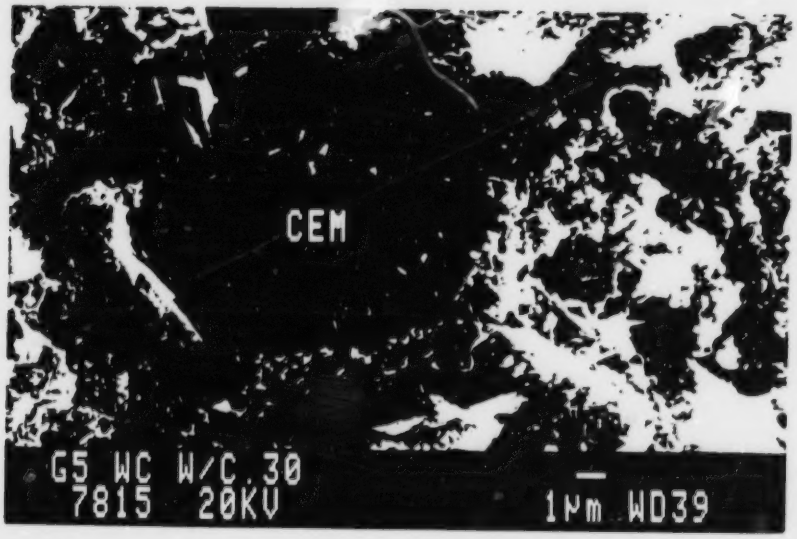

Fig. 54 Reaction rim around a cement particle

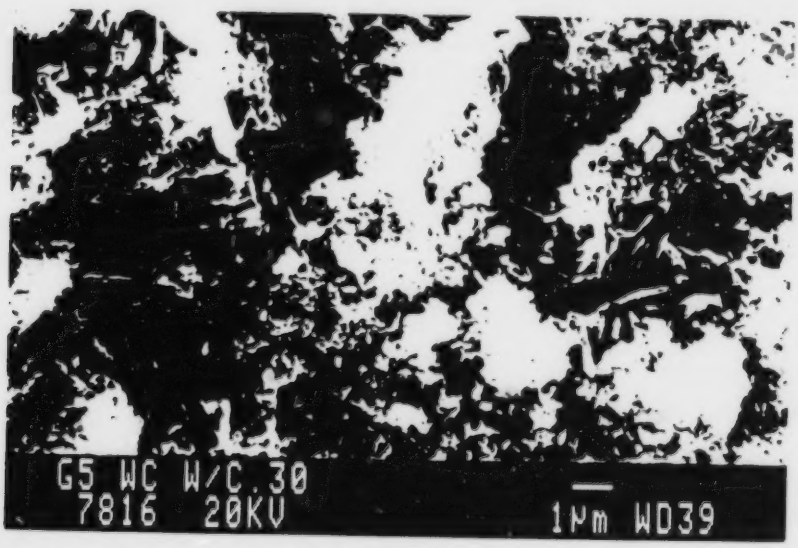

Fig. 55 Porous transition zone

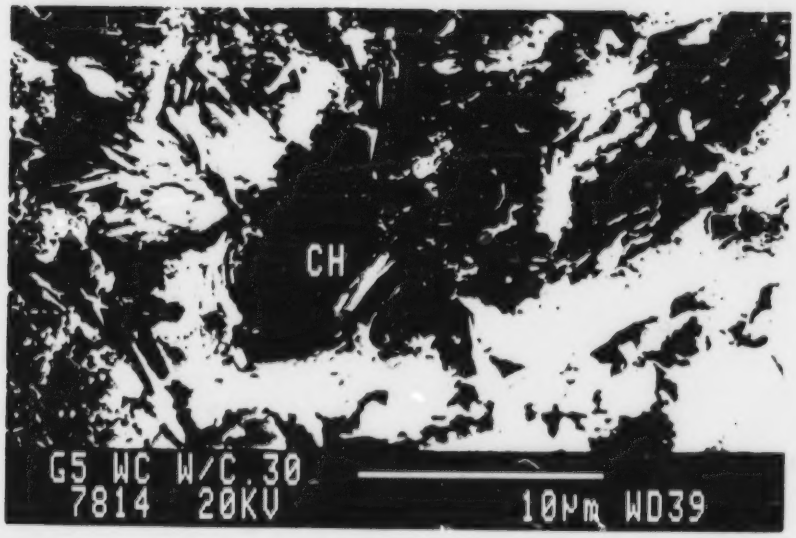

Fig. 56 Platy CH crystals and ettringite needles in the transition zone

G8 concrete, with 10% SF, air cured, W/C+SF = 0.30

The paste is mostly dense (Fig. 57), except that a number of vacant sockets are present in parts of the paste (Figs. 58 and 59). Similar features are also observed at the paste-aggregate interface (Figs. 60 and 61). Though CH is present in some parts of the interface, it is not as oriented as its water cured counterpart concrete, G7. Partly hydrated cement grains with reaction rims, as seen in Figure 57, are present in the paste. The stacking morphology of CH seen previously in G7 is absent. The transition zone is granular, that gives it a porous appearance (Fig. 62). Some small irregular particles of CH are constituents of this granular feature.

G8 Concrete

Fig. 57 Dense paste. A partly hydrated cement grain with reaction rim can also be seen

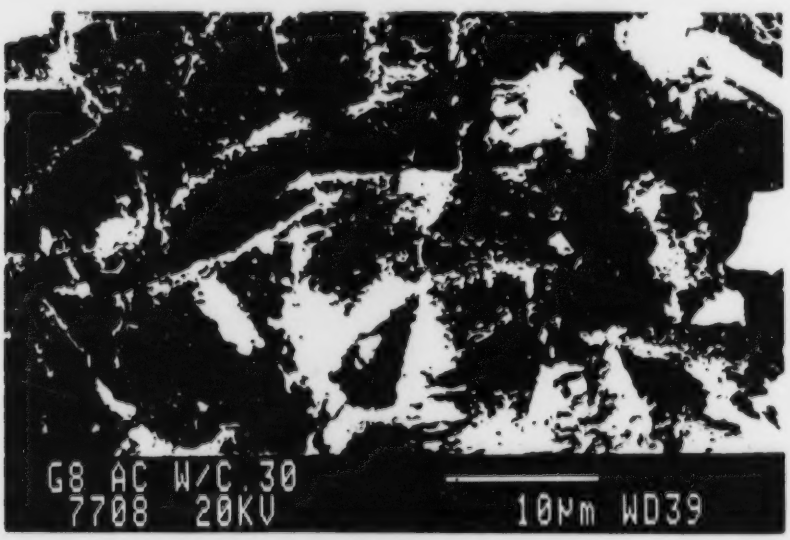

Fig. 58 Dense paste containing a number of empty sockets

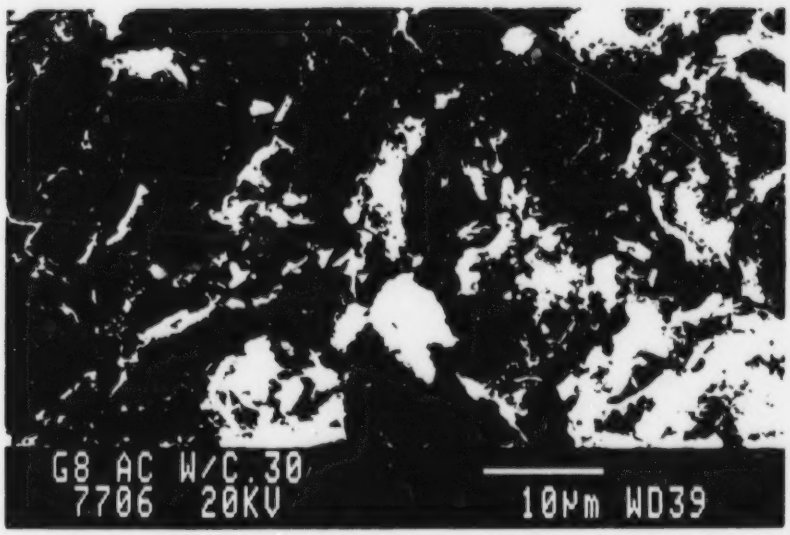

Fig. 59 Another view of the paste showing empty spaces

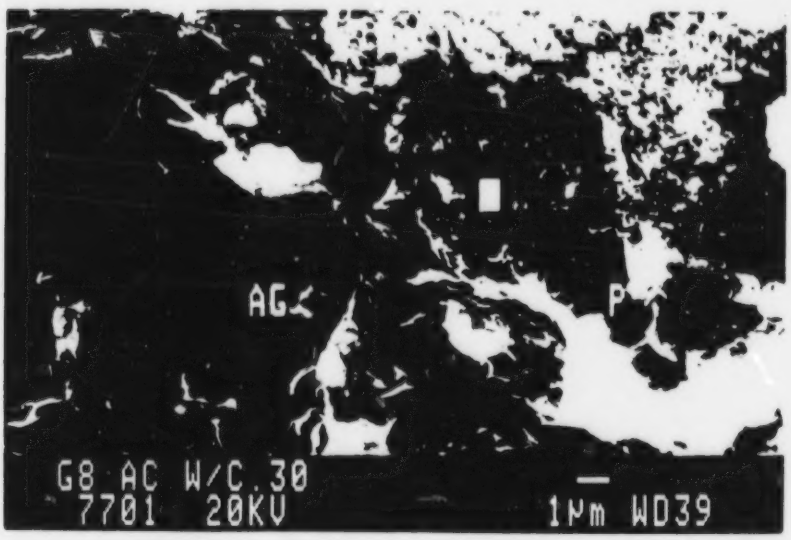

Fig. 60 Porous paste-aggregate interface

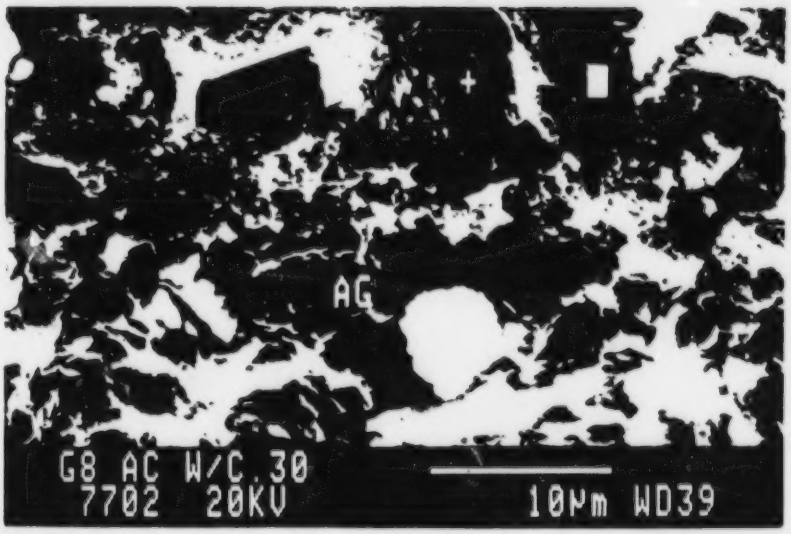

Fig. 61 Same

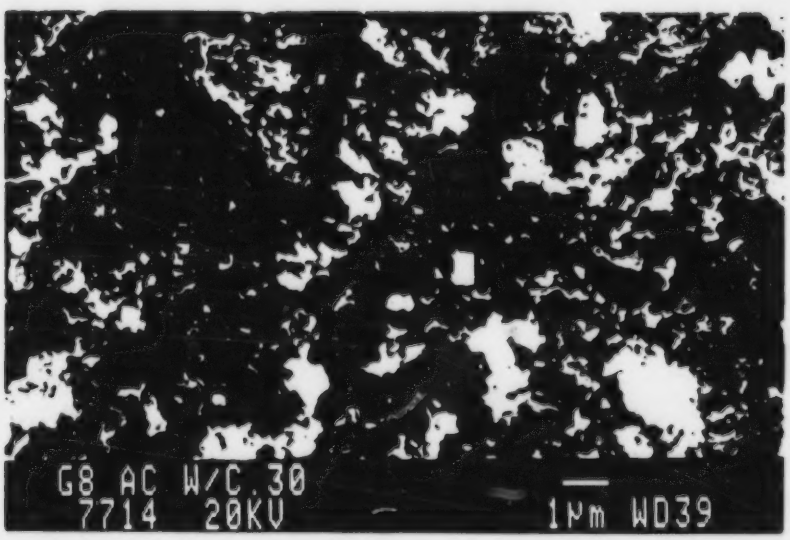

Fig. 62 Granular feature at the transition zone. Some of them are tiny CH crystals

G6 control concrete, without silica fume, air cured, W/C = 0.30

As in G2 control concrete (W/C = 0.25), C-S-H is less dense (Fig. 63) in the paste. Fissures are present around hydrating cement grains (Fig. 64). Fissures also become visible at the CH: C-S-H boundary (Fig. 65). Indistinct stacking of CH is present (Fig. 66).

Oriented CH crystals have developed at the paste-aggregate interface (Figs. 67 and 68). Here also one sees fissures at the CH: C-S-H junction (Fig. 68).

The transition zone, which is porous, comprises C-S-H, CH and hydrating cement grains (Figs. 69 and 70).

G6 Concrete

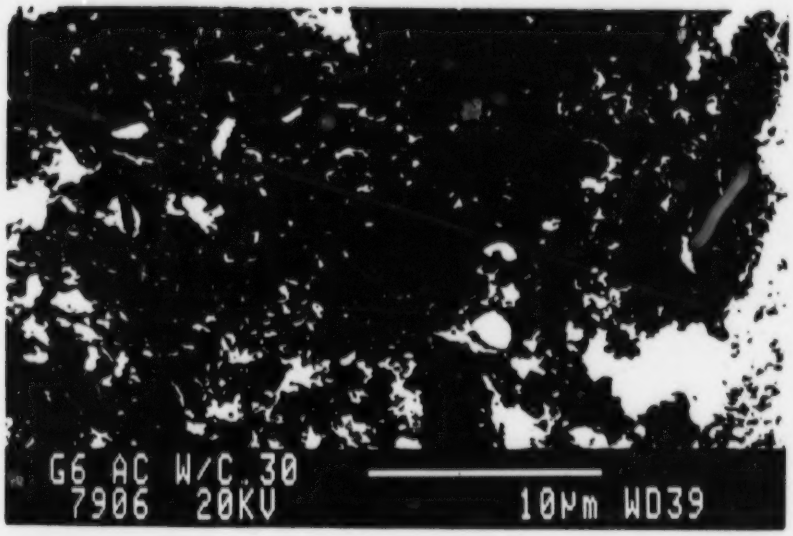

Fig. 63 Less dense paste

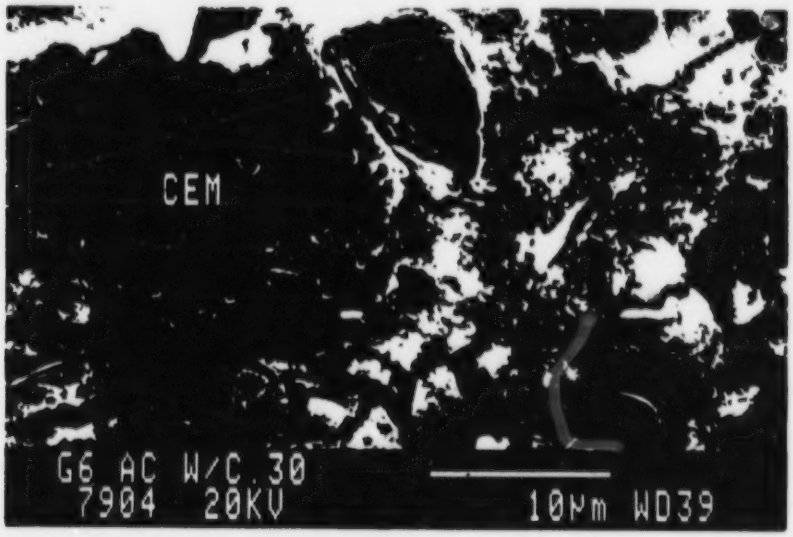

Fig. 64 A hydrating cement grain with fissures around it

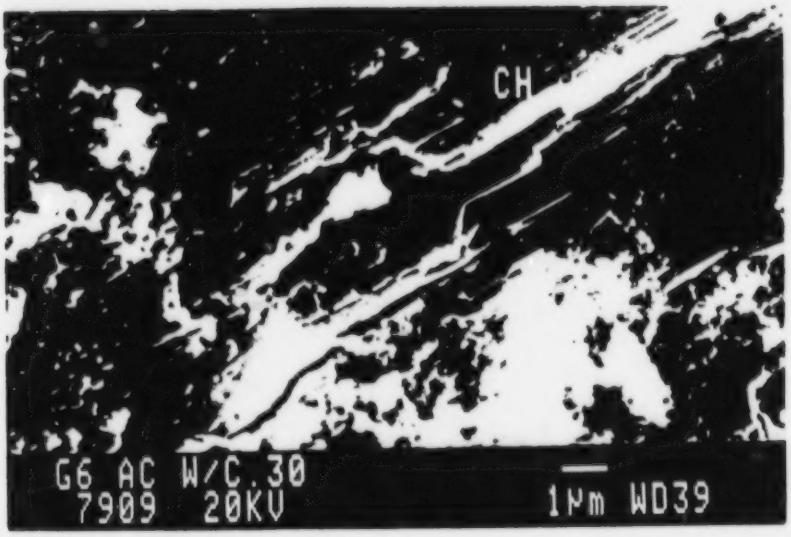

Fig. 65 Large CH crystals with a fissure along the boundary

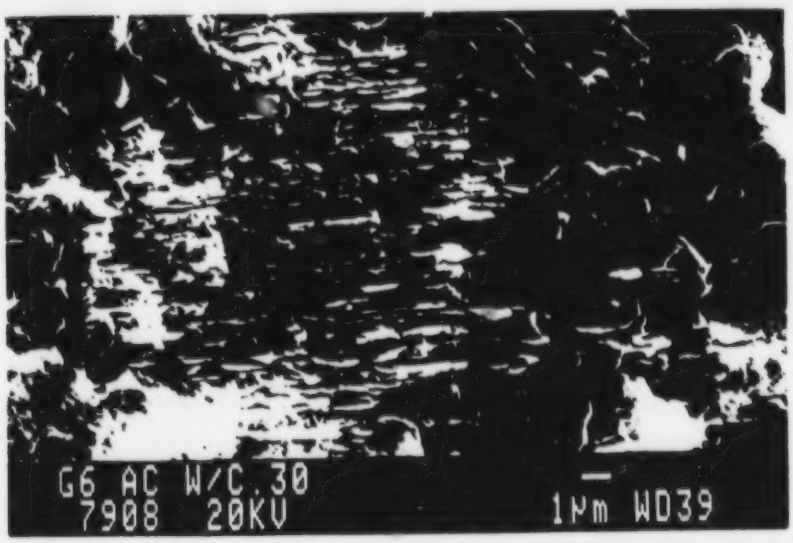

Fig. 66 Indistinct stacked CH crystals

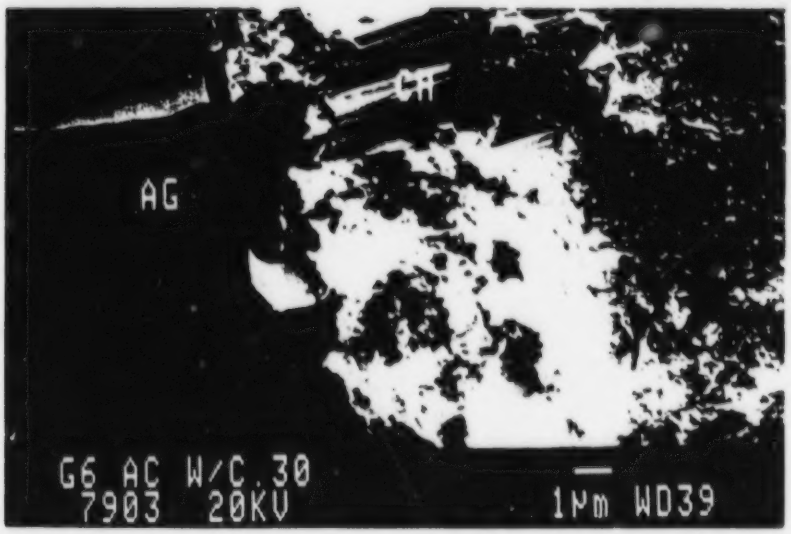

Fig. 67 Oriented CH crystals at the paste-aggregate interface

Fig. 68 Same feature. A fissure along its boundary can be seen

Fig. 69 Porous transition zone with a hydrating cement grain and C-S-H

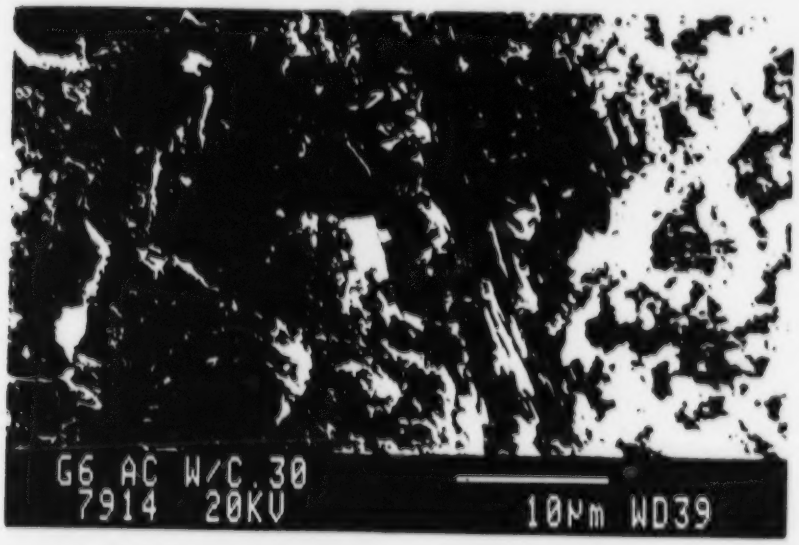

Fig. 70 Porous transition zone with oriented CH crystals and C-S-H

G11 concrete, with 10% SF, water cured, W/C+SF = 0.40

Increase in W/C ratio does not appear to have affected the paste microstructure significantly. The paste is still dense, except the pores are larger (Figs. 71 and 72). This, however, can be a combined effect of increasing dosage of air entraining agent and water in the concrete.

Massive CH crystals have formed, but still have not acquired the perfect geometry (Figs. 73 and 74). Fissures around hydraitng cement grains are present (Fig. 75). In general cement hydration has progressed much further in this concrete (as shown in Fig. 76), because of higher W/C ratio. The paste-aggregate bonding is strong (Fig. 77). The transition zone occasionally shows massive CH (Fig. 78), but is mostly C-S-H (Fig. 79). The porosity of this zone is not very different from that of the paste (Figs. 79 and 80).

G11 Concrete

Fig. 71 Dense paste, but pores are larger in diameter

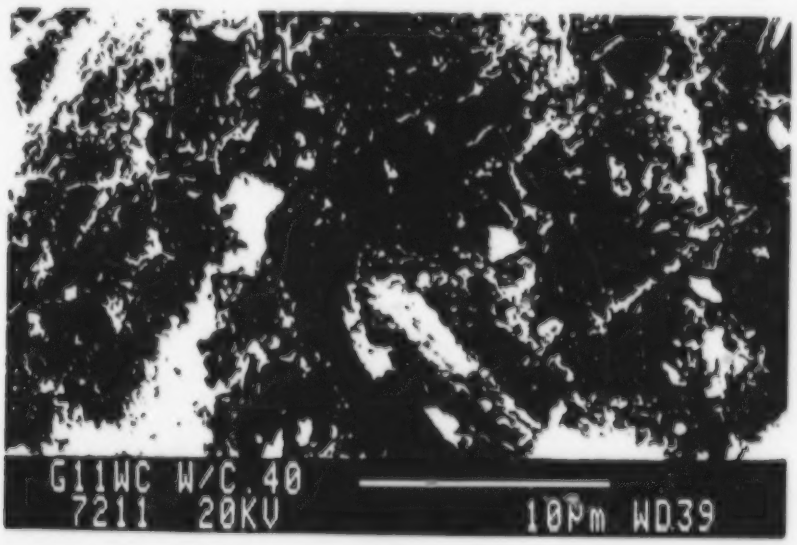

Fig. 72 Same

Fig. 73 Massive CH, geometrically not well developed, in the paste

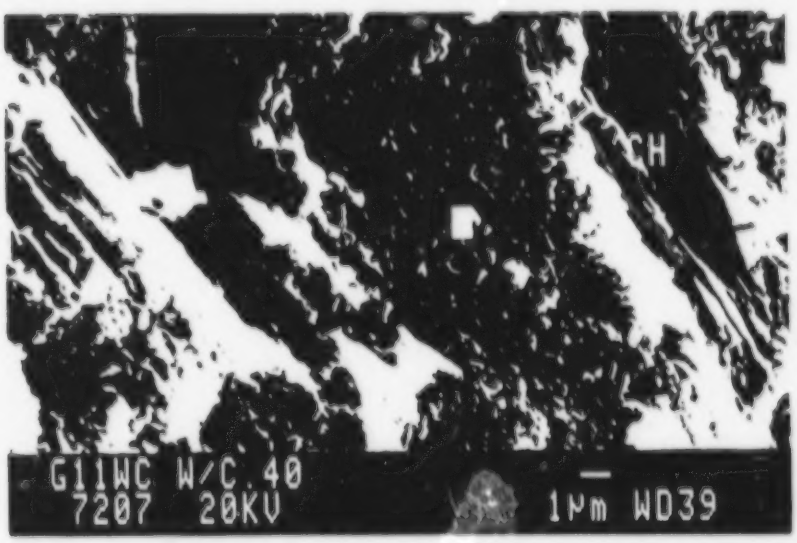

Fig. 74 Same

Fig. 75 A partly hydrating cement grain with a fissure around it

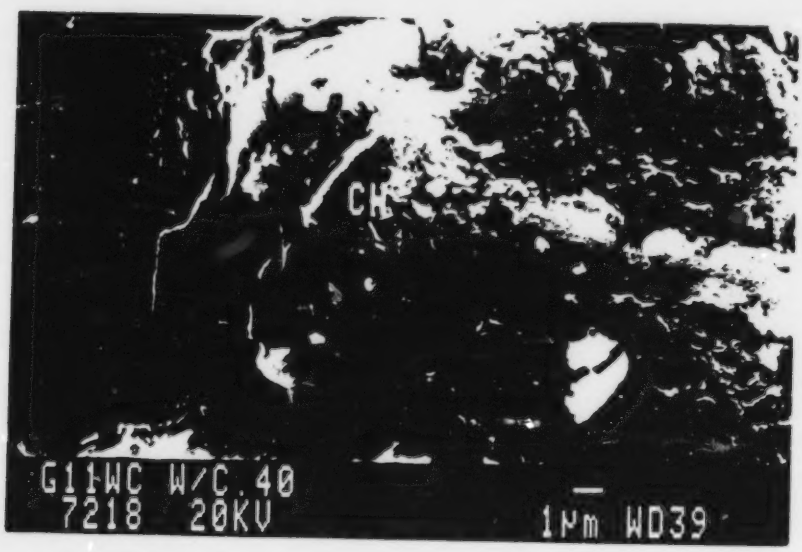

Fig. 76 A cement grain in a much more advanced state of hydration

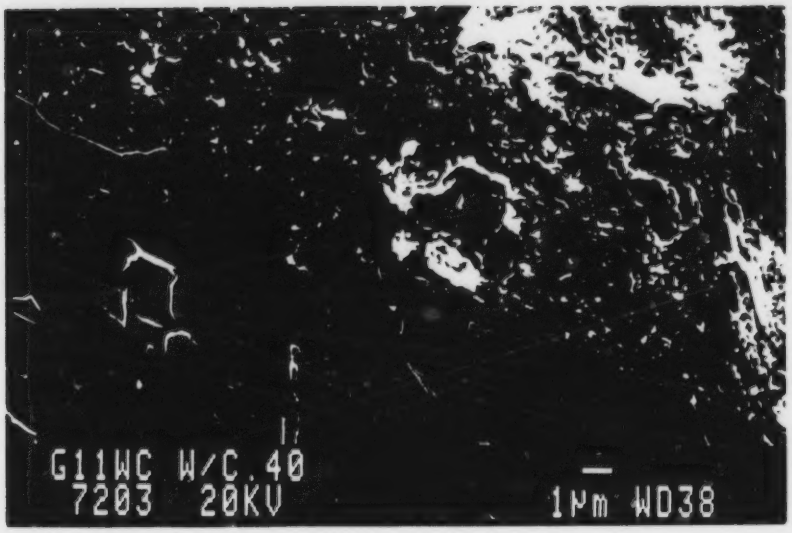

FIg. 77 Strong paste-aggregate bonding

Fig. 78 Massive oriented CH crystals in the transition zone

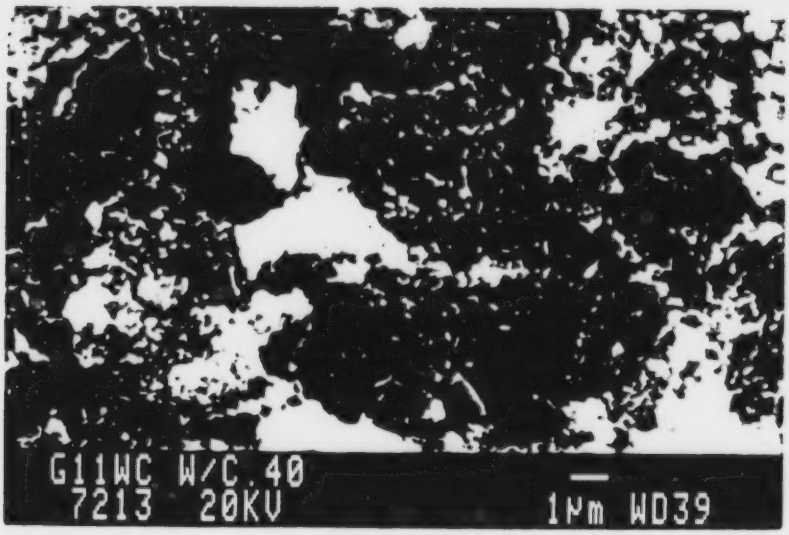

Fig. 79 Transition zone comprising C-S-H, and showing porosity

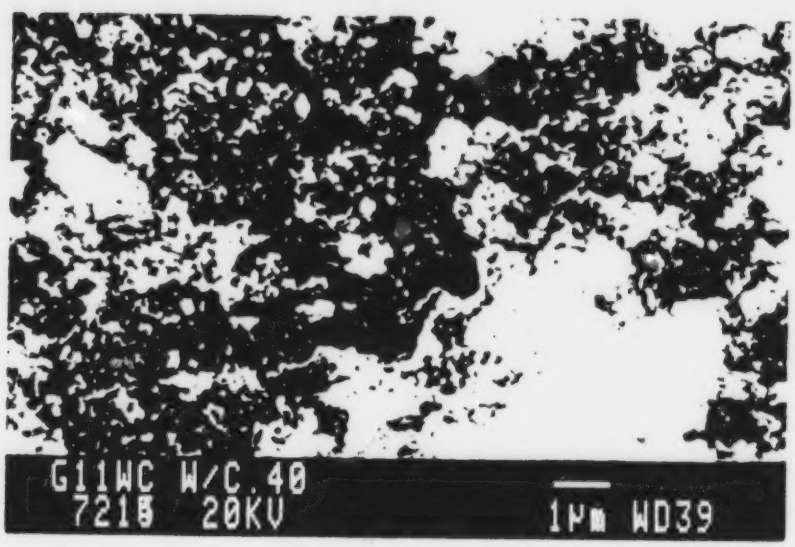

Fig. 80 Dense transition zone

G9 control concrete, without silica fume, water cured, W/C = 0.40

Compared to the G11 silica fume concrete with the same W/C ratio, the paste is less dense in this control concrete (Figs. 81 and 82). Non-negligible amount of ettringite needles has formed in the voids (fig. 83). Massive CH, not very well crystallized geometrically is present (Fig. 84). Some parts of the paste-aggregate interface contain small oriented CH crystals (Fig. 85). Other interfaces, however, comprise C-S-H (Fig. 86). In some of the vacant spaces at the interface, ettringite can be seen (Fig. 87).

The transition zone is characterized by platy CH crystals (Fig. 88) and Type I C-S-H (fig. 89). The latter gives it higher porosity in this zone. A magnified view of this type of C-S-H is shown in Figure 90.

G9 Concrete

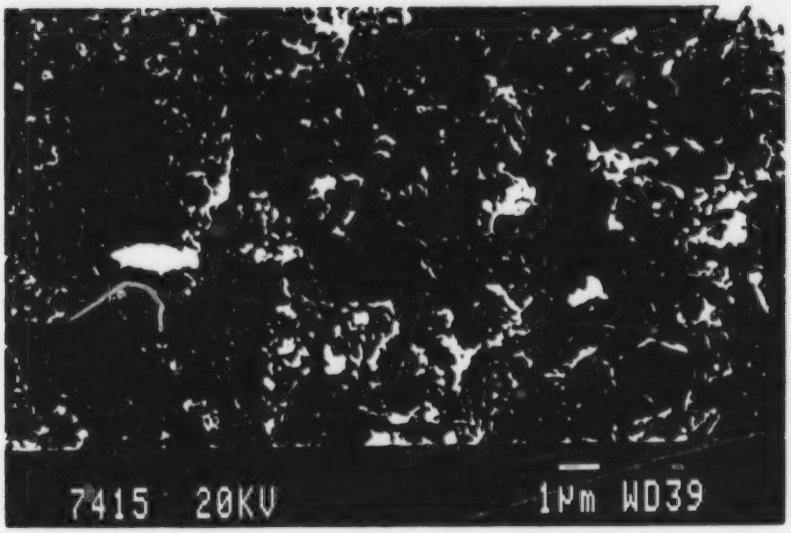

Fig. 81 Porous paste

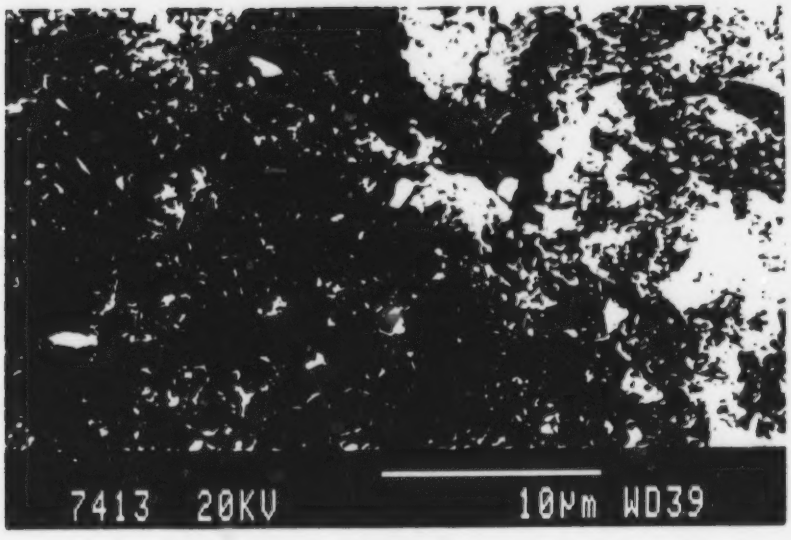

Fig. 82 Same

Fig. 83 Ettringite needles in a void

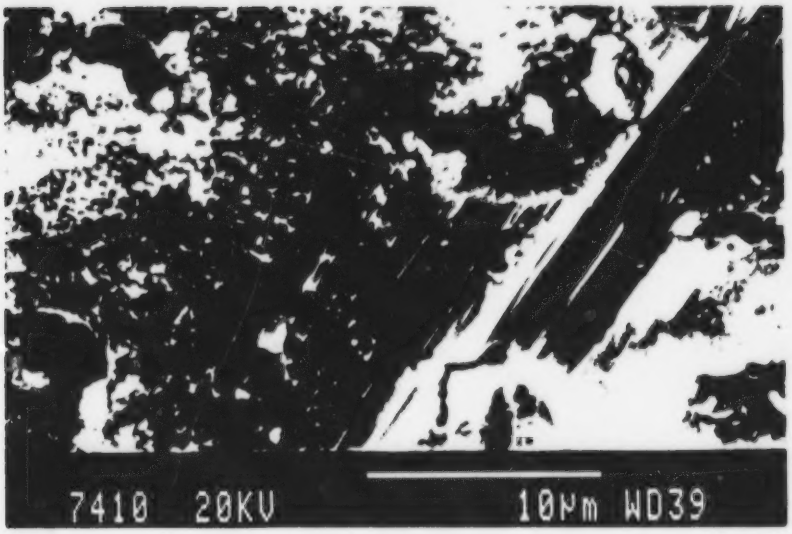

Fig. 84 Massive CH in the paste

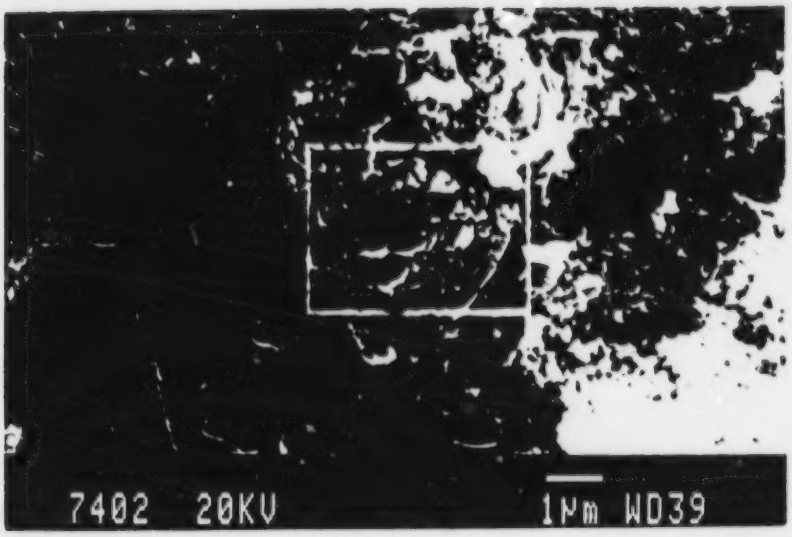

Fig. 85 CH (boxed) at the paste-aggregate interface

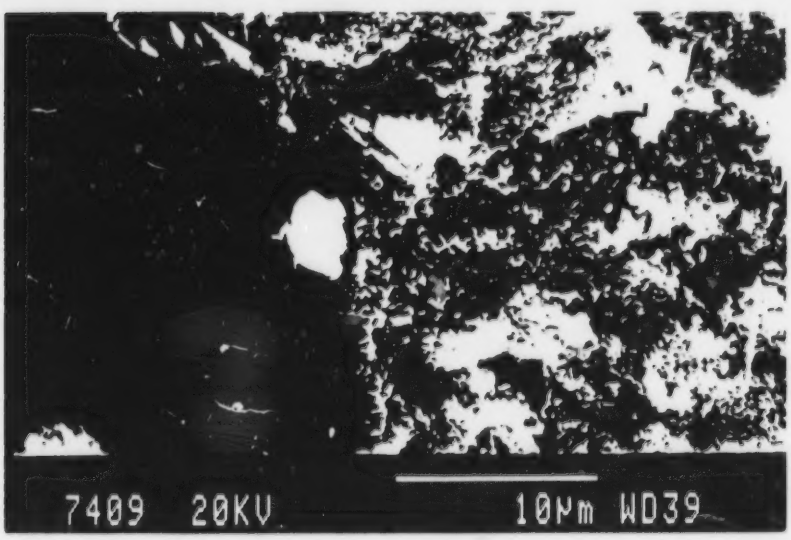

Fig. 86 C-S-H at another interface

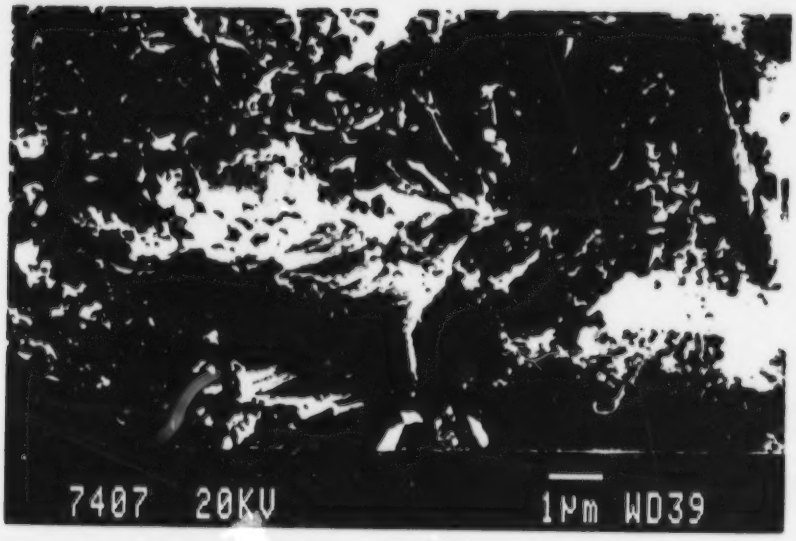

Fig. 87 Ettringite needles at an interface

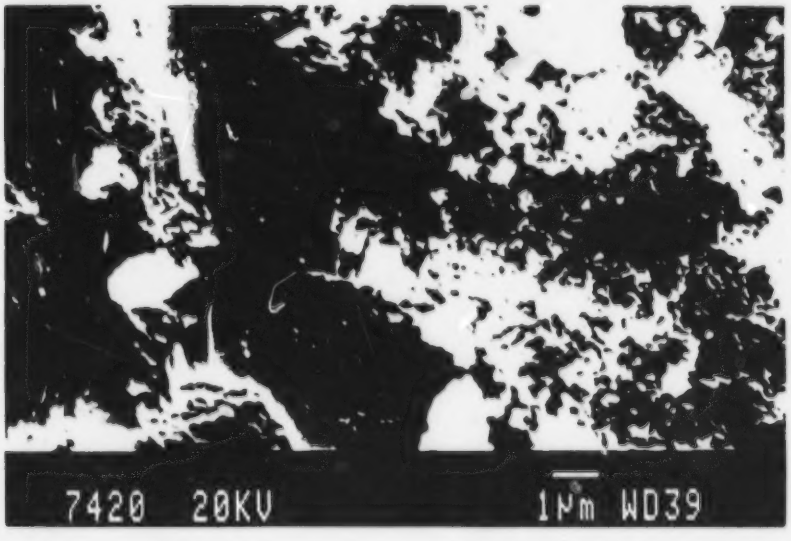

Fig. 88 Platy CH in the transition zone

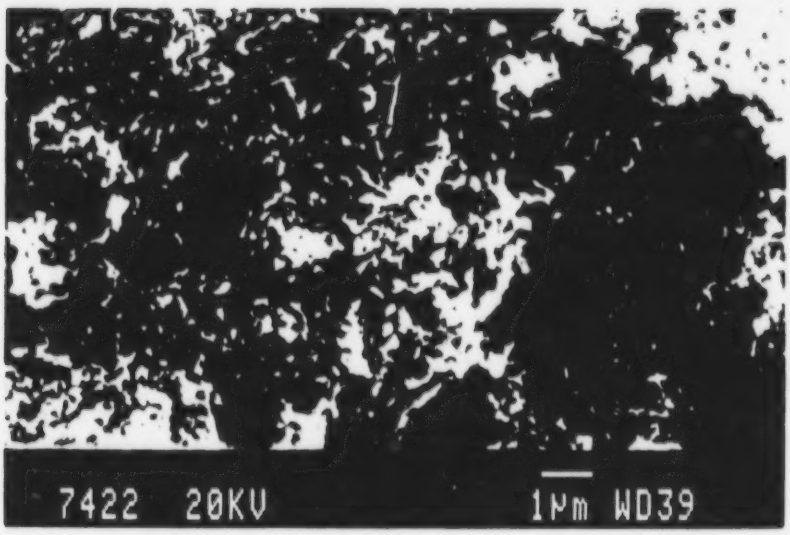

Fig. 89 Type I C-S-H in the transition giving rise to higher porosity

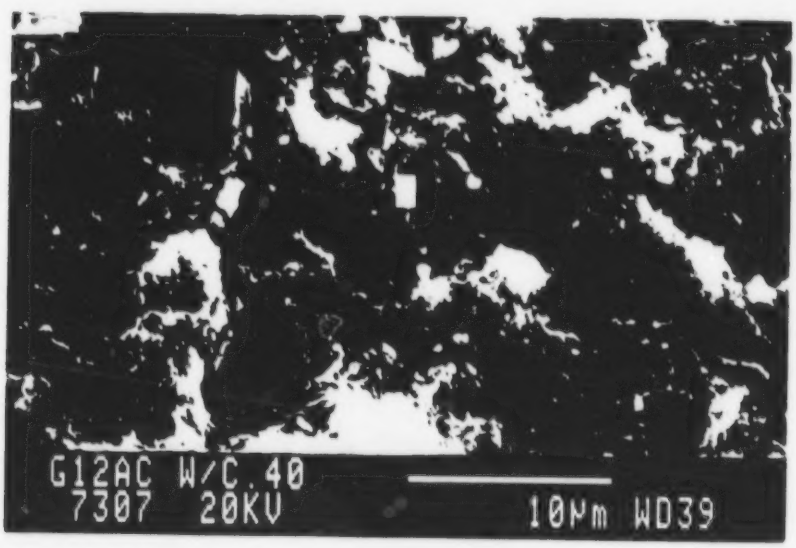

Fig. 90 A magnified view of Type I C-S-H

G12 concrete with 10% SF, air cured, W/C+SF = 0.40

The paste is dense (Fig. 91) as in G11 silica fume concrete of same W/C+S ratio. Partly hydrated cement grains are present (Fig. 92). Massive CH has developed in the paste (Fig. 93).

The paste-aggregate interface is composed of Type I C-S-H and small oriented CH crystals (Figs. 94 and 95). This type of C-S-H increases the porosity at the interface. The transition zone also shows higher porosity (Fig. 96). In parts of this zone, platy CH crystals can be seen (Fig. 97).

G12 concrete

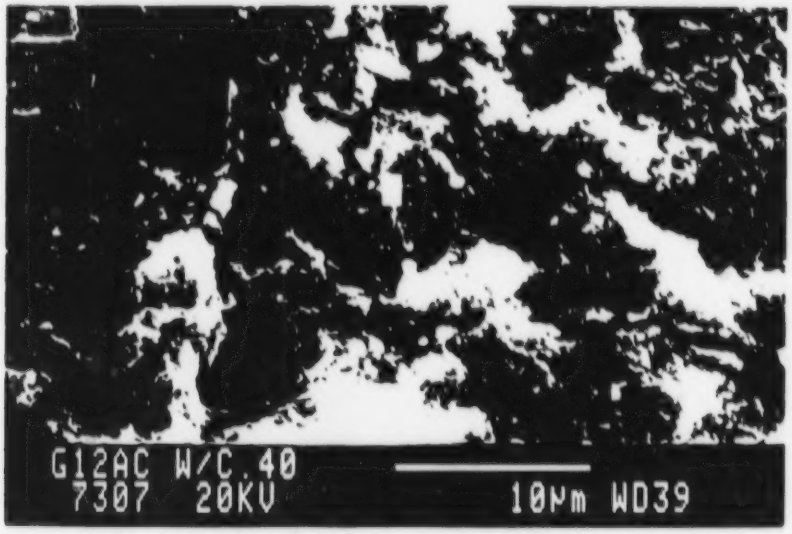

Fig. 91 Dense paste

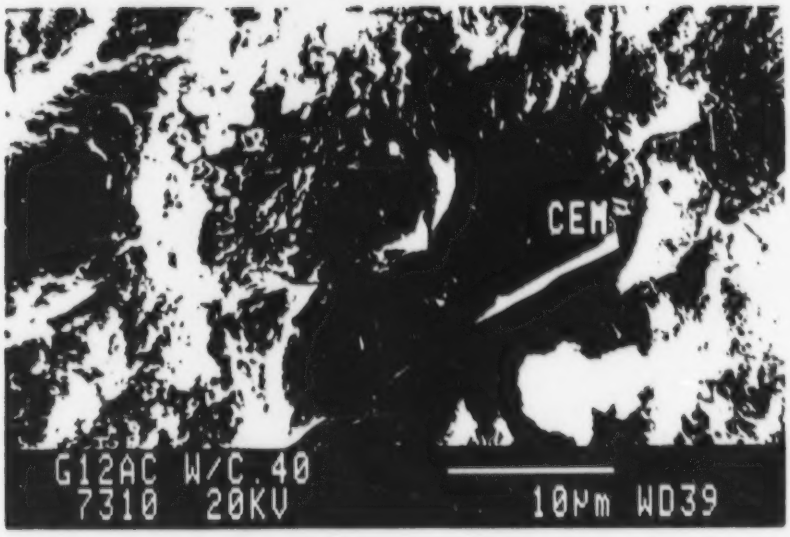

Fig. 92 Partly hydrated cement grain in this dense paste

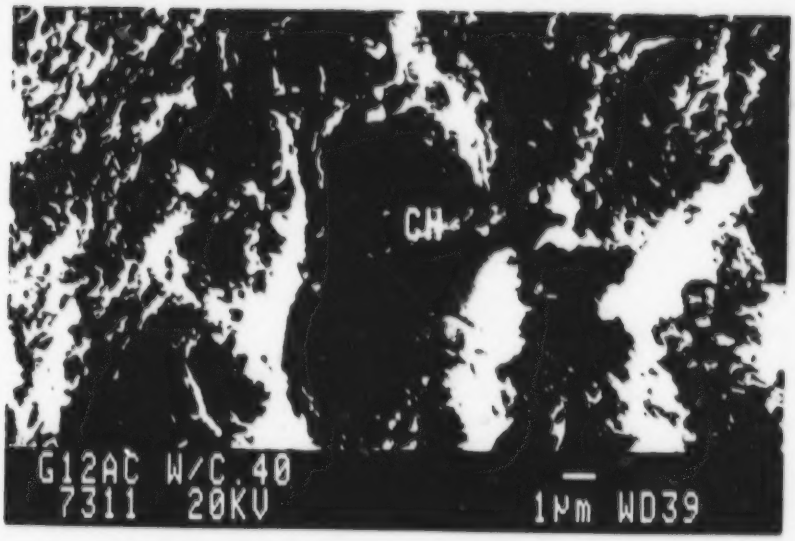

Fig. 93 Massive CH in the paste

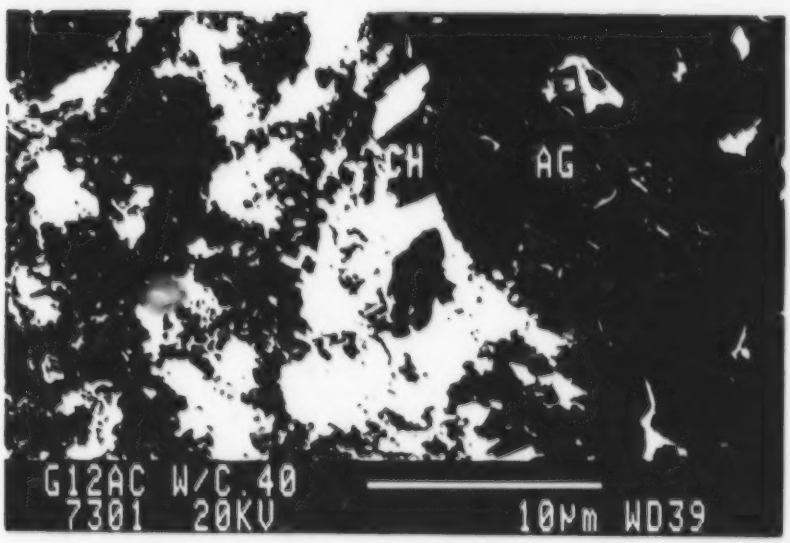

Fig. 94 Small oriented CH crystals and Type I C-S-H at the paste-agregate interface

Fig. 95 Type I C-S-H at the interface

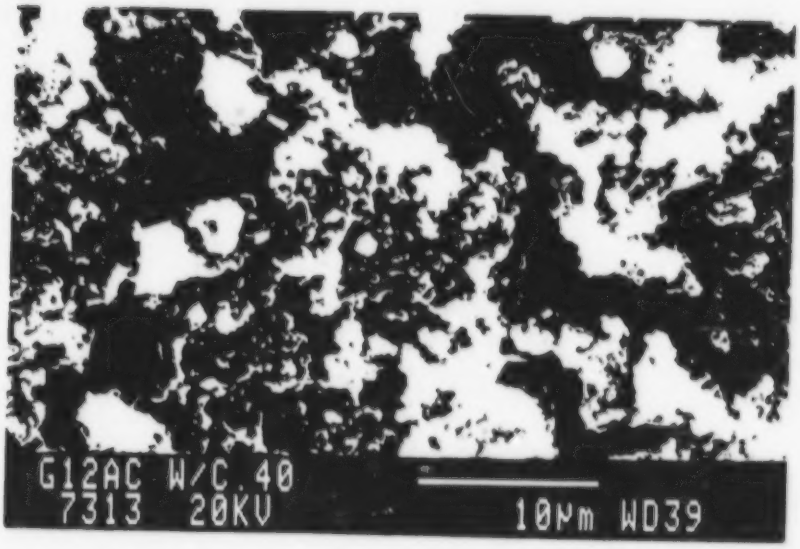

Fig. 96 Porous transition zone

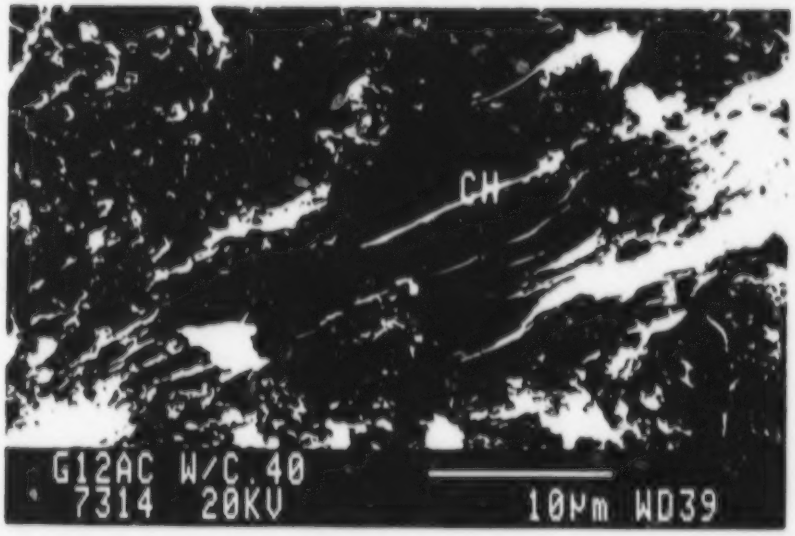

Fig. 97 Platy CH crystals in the transition zone

G10 control concrete, without SF, air cured, W/C = 0.40

The paste is distinctly porous comprising Type I C-S-H (Fig. 98). Ettringite is also associated with it (Fig. 99). Massive CH crystals are present (Fig. 100).

The paste-aggregate interface shows weakening with numerous tiny irregular crystals of CH (Figs. 101 and 102) that also increases the porosity of the interface.

In the transition zone massive CH as seen in the paste, are common (Fig. 103). The transition zone is porous due to the presence of Type I C-S-H.

G10 Concrete

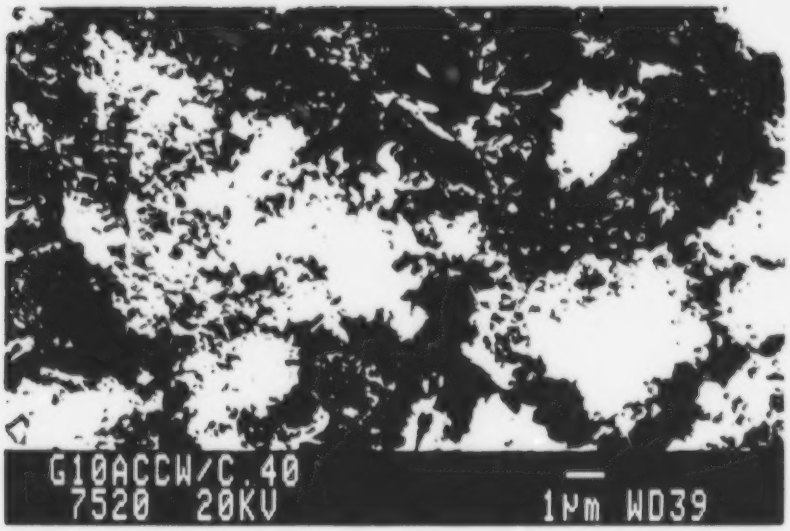

Fig. 98 Type I C-S-H in the paste which makes the paste porous

Fig. 99 Ettringite needles in the paste

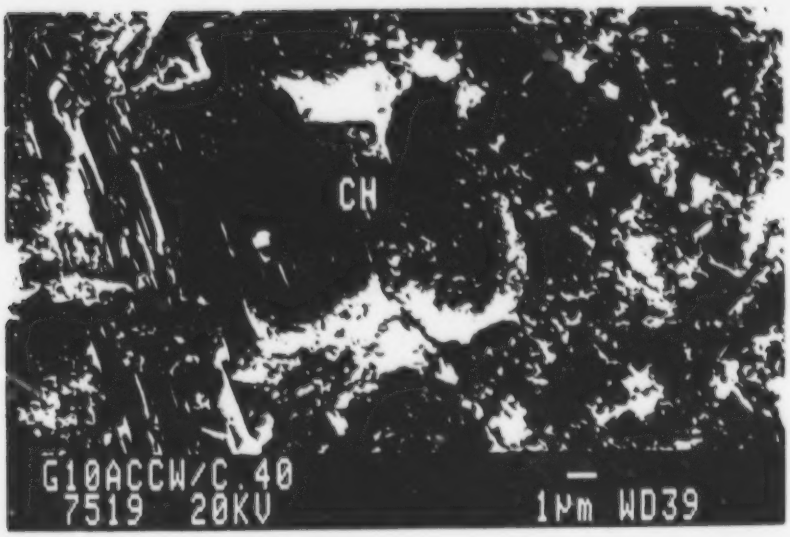

Fig. 100 Massive CH crystals in the paste

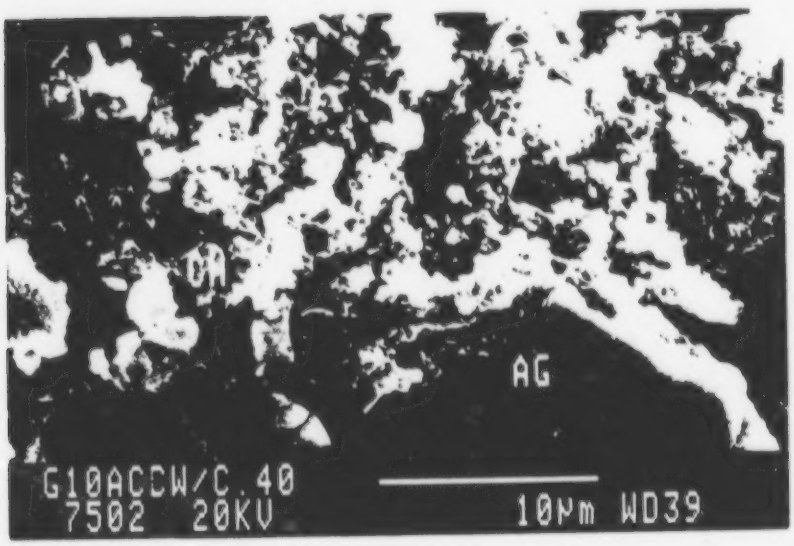

Fig. 101 Tiny irregular CH crystals at the paste-aggregate interface

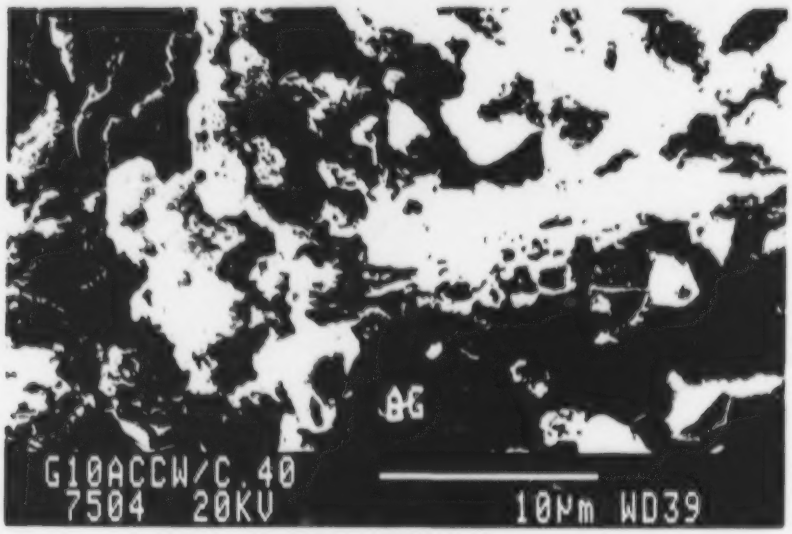

Fig. 102 Same

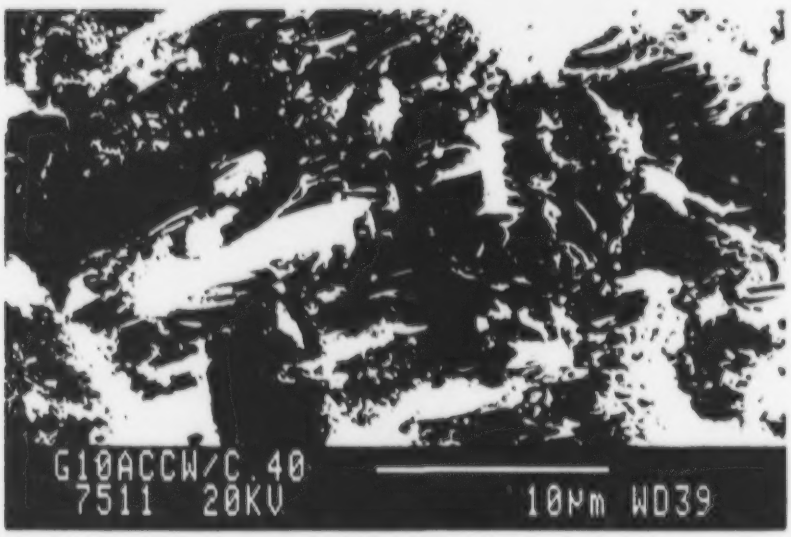

Fig. 103 Massive CH crystals in the transition zone

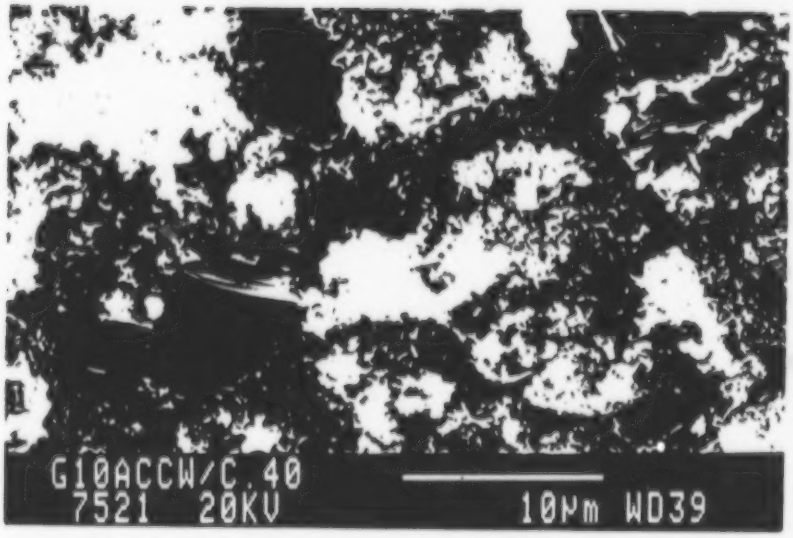

Fig. 104 Type I C-S-H and CH in the transition zone

(ii) XRDA

The plots for the CH peak at 18.04° 2θ for all the concretes is shown in Figure 105a-c. The integrated intensities of this peak are shown in the histogram mode in Figure 106. It is clear that CH increases with increase in water to solid ratio for both sets of concretes, with and without SF. However, in the case of the air cured concretes this trend is not so obvious. This can lead to certain uncertainties when interpreting the results.

In order to minimize the effect of experimental errors, variance analysis (2) was performed. This enabled to study precisely the difference in the quantity of CH generated as a function of three variables, and comment on the significance of each of these influencing factors.

The three variables that were used for interpreting the results are:

(i) W/C+SF, water-to-solid ratio

(ii) Curing method

(iii) SF/C+SF, replacement of cement by SF

The scheme is shown in Table 3 below.

Table 3

Factor		Level		
		1	2	3
A	W/C+SF	0.25	0.30	0.40
B	Curing	water	air	
C	SF/C+SF	0	0.10	

The results of integrated intensity of the CH peak at 18.04°2θ and peak height at 34.08°2θ are given in Table 4. The factors and levels are also listed in this table.

Table 4

Specimen No.	Factor			I_I 18.04°2θ*	P_h (absolute) 34.08°2θ**
	A	B	C		
1	1	1	1	11873	426
2	1	2	1	9273	356
3	1	1	2	4070	129
4	1	2	2	5153	178
5	2	1	1	15834	722
6	2	2	1	10674	411
7	2	1	2	5071	201
8	1	2	2	5070	182
9	3	1	1	16229	579
10	3	2	1	9062	365
11	3	1	2	6536	271
12	3	2	2	6873	237

* Integrated intensity ** Peak height

Since measurement of I_I and P_h show identical trends, only the I_I values were used in the calculations.

The interactions between the factors that affect the formation of CH are plotted in figures 107a-c. The summarized analyses are shown in Figure 108.

From Figure 107a it is evident that the amount of CH formed in the air cured concretes is definitely lower at all levels of W/C+SF, irrespective of the presence/absence of SF. The amount of CH in the air cured concretes increases linearly with increase in W/C

ratio. This is more rapid between W/C = 0.25 to 0.30 and more singificant in the water cured ones.

Figure 107b clearly shows lower amount of CH formation in the SF concretes at all three W/C+SF ratios. However, CH does increase slightly with the W/C+SF ratio. One must take note of the fact that the amount of cement in the concrete mixes decrease progressively from W/C = 0.25 to 0.40 (Table 2). Since the quantity of SF is constant at 10%, its consumption capacity of CH is not likely to increase with W/C+SF ratio. On the other hand, despite gradual decrease in cement quantity the formation of CH increases with increase in water content in the concrete. It signifies that cement hydration (or CH formation) is faster than its consumption by SF as a functin of W/C+SF ratio. The trend of the plot for concretes without silica fume is seen to be non-linear. A steep rise in CH formation can be observed between 0.25 and 0.30 W/C ratio. Between 0.30 and 0.40 no rise is seen to occur. It can be said that at W/C = 0.25, the amount of water available for CH to form from the hydration of cement particles is so low that despite the highest amount of cement in these concretes, CH formed is lower than at W/C = 0.30, although the latter contains lesser cement. At the other extreme is the 0.40 W/C concrete with so low cement quantity, that the amount formed does not exceed that of W/C = 0.30. Nevertheless, CH formation in the non-silica fume concretes is distinctly higher than the SF concretes at all W/C ratios.

In Figure 107c, one observes a strong two-factor interaction (between factor B and C). CH formed in air cured concretes without SF is significantly lower than their water cured counterparts. This effect does not show up in the SF concretes. As a matter of fact, air cured concretes show slightly higher CH content than the water cured ones, suggesting lower consumption of CH in the air cured concretes.

The summary of the effects and significance of the influencing factors shown in Figure 108 is self explanatory.

Elevated level of CH in water cured concretes indicates the posibility of increased mobility of ions in the hydrating system. It is unlikely that in such dense pastes as these, permeation of water would take place during curing to enable hydration to continue. Loss of moisture in the air cured concretes at early age can cause shrinkage consequently reducing space for crystal growth. This would account for lower CH formation.

ANALYSIS OF EMPA RESULTS

The Ca versus Si counts plotted in Figure 110 clearly shows some scattering, that is significantly larger in the transition zone. Closer examination of the bulk paste analysis plot indicates data points in quadrant A to constitute mainly the silica fume concretes (G3, G4, G6, g8, G11 and G12).

From the results of F-test (Fig. 111) it is evident that the Ca/Si ratio of C-S-H in the paste as well as the transition zone decreases with the addition of silica fume.

Air-cured concretes have a slightly higher Ca/Si ratio in the paste and the transition zone than their water cured counter-parts.

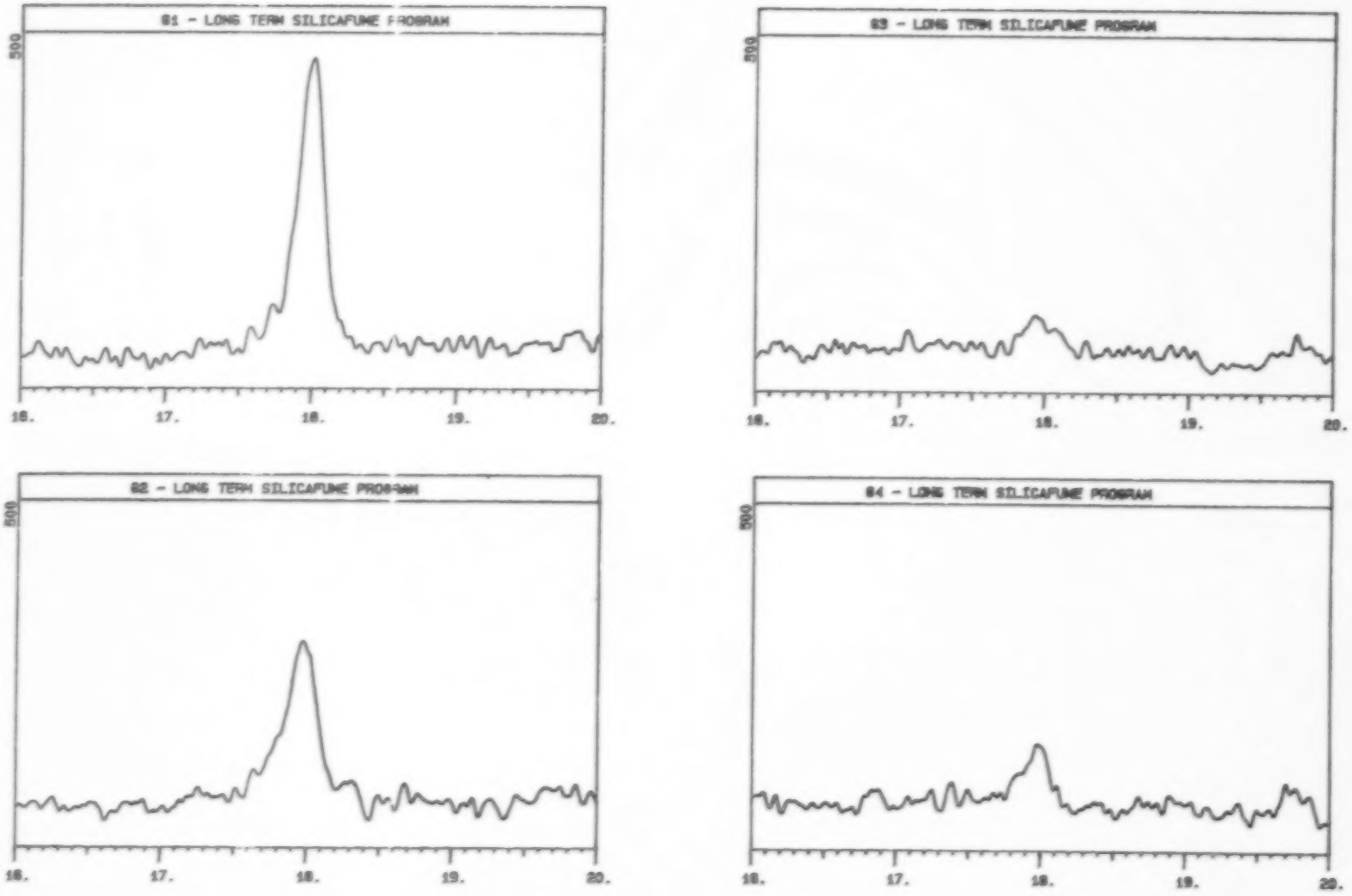
01 - LONG TERM SILICAFUME PROGRAM
500
16.
17.
18.
19.
20.
03 - LONG TERM SILICAFUME PROGRAM
500
16.
17.
18.
19.
20.
02 - LONG TERM SILICAFUME PROGRAM
500
16.
17.
18.
19.
20.
04 - LONG TERM SILICAFUME PROGRAM
500
16.
17.
18.
19.
20.

Fig. 105a

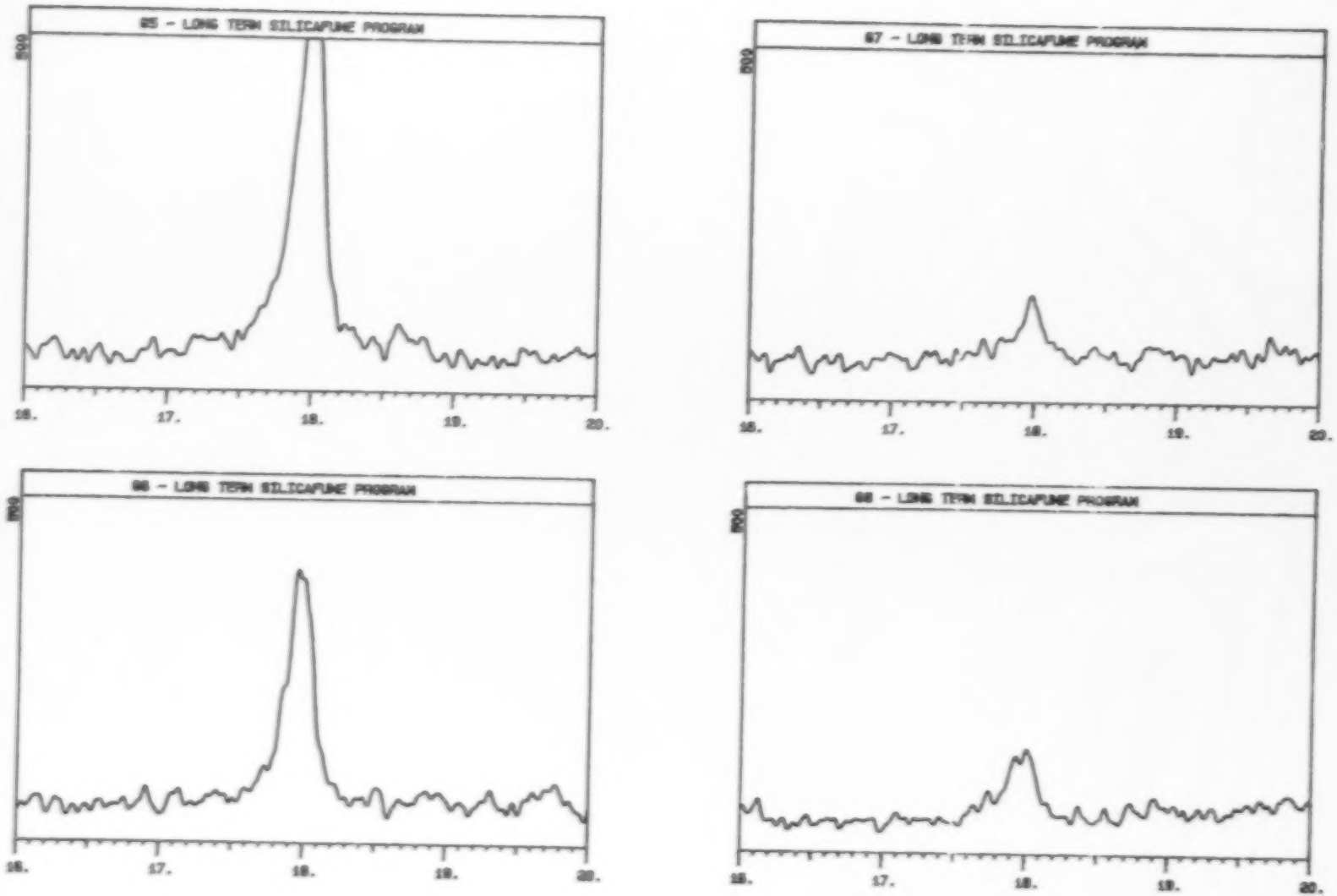
65 - LONG TERM SILICAFUME PROGRAM
500
16.
17.
18.
19.
20.
67 - LONG TERM SILICAFUME PROGRAM
500
16.
17.
18.
19.
20.
66 - LONG TERM SILICAFUME PROGRAM
500
16.
17.
18.
19.
20.
68 - LONG TERM SILICAFUME PROGRAM
500
16.
17.
18.
19.
20.

Fig. 105b

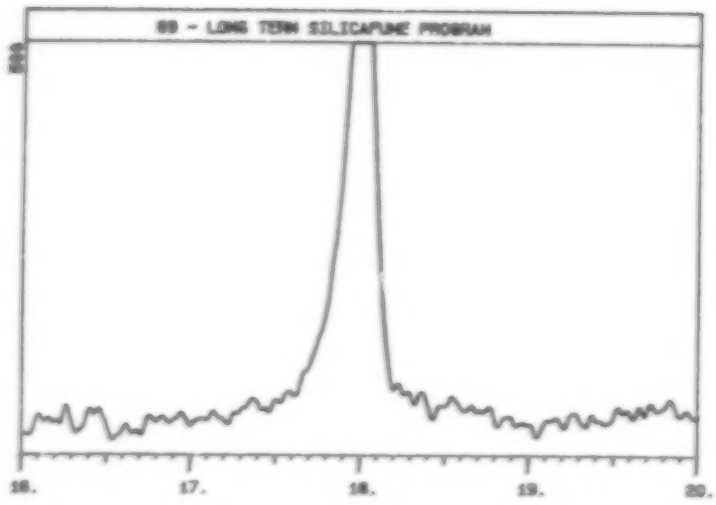
09 - LONG TERM SILICAFUME PROGRAM
16.
17.
18.
19.
20.

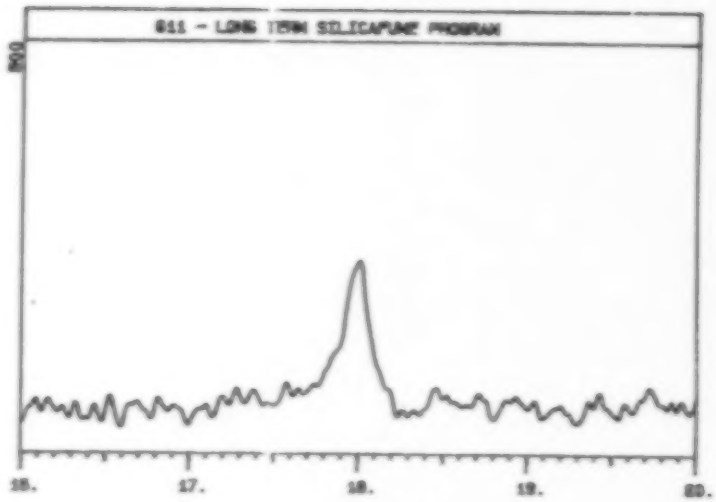
011 - LONG TERM SILICAFUME PROGRAM
16.
17.
18.
19.
20.

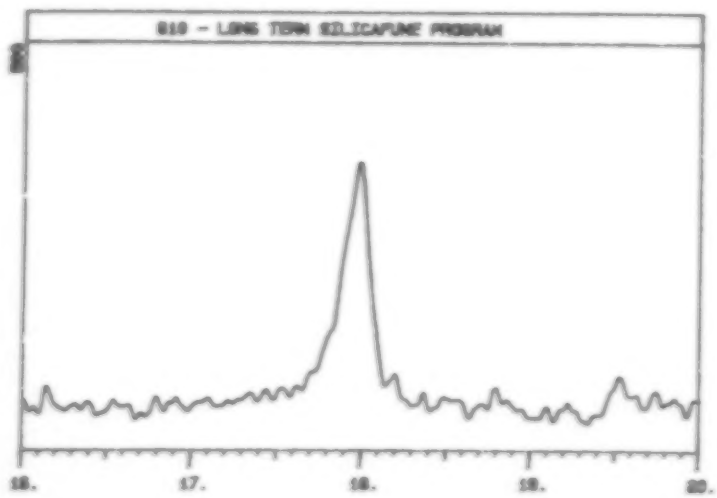
010 - LONG TERM SILICAFUME PROGRAM
16.
17.
18.
19.
20.

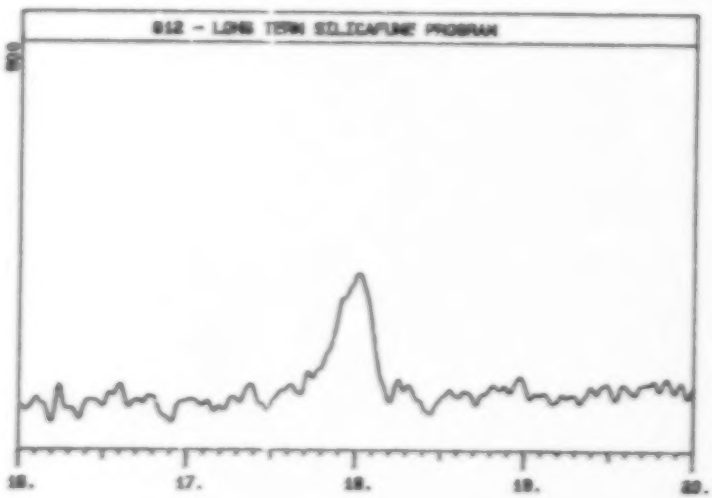
012 - LONG TERM SILICAFUME PROGRAM
16.
17.
18.
19.
20.

Fig. 105c

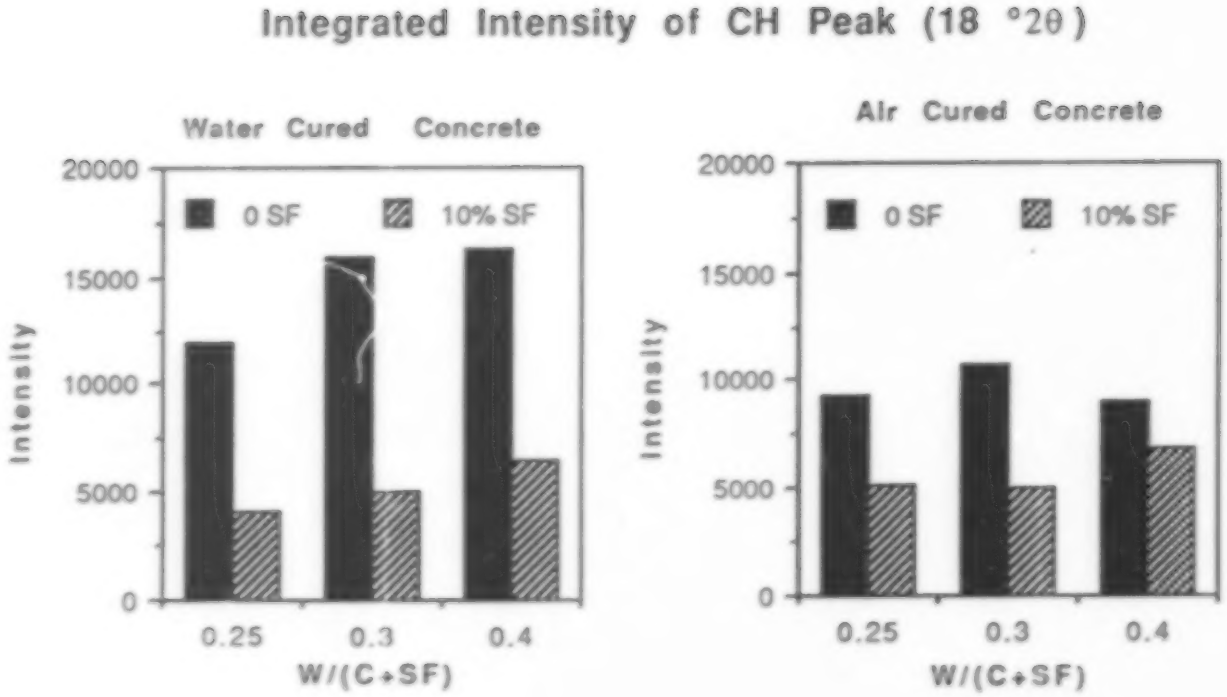

Fig. 106 Histograms of I_I of the CH peak at 18.04° 2θ

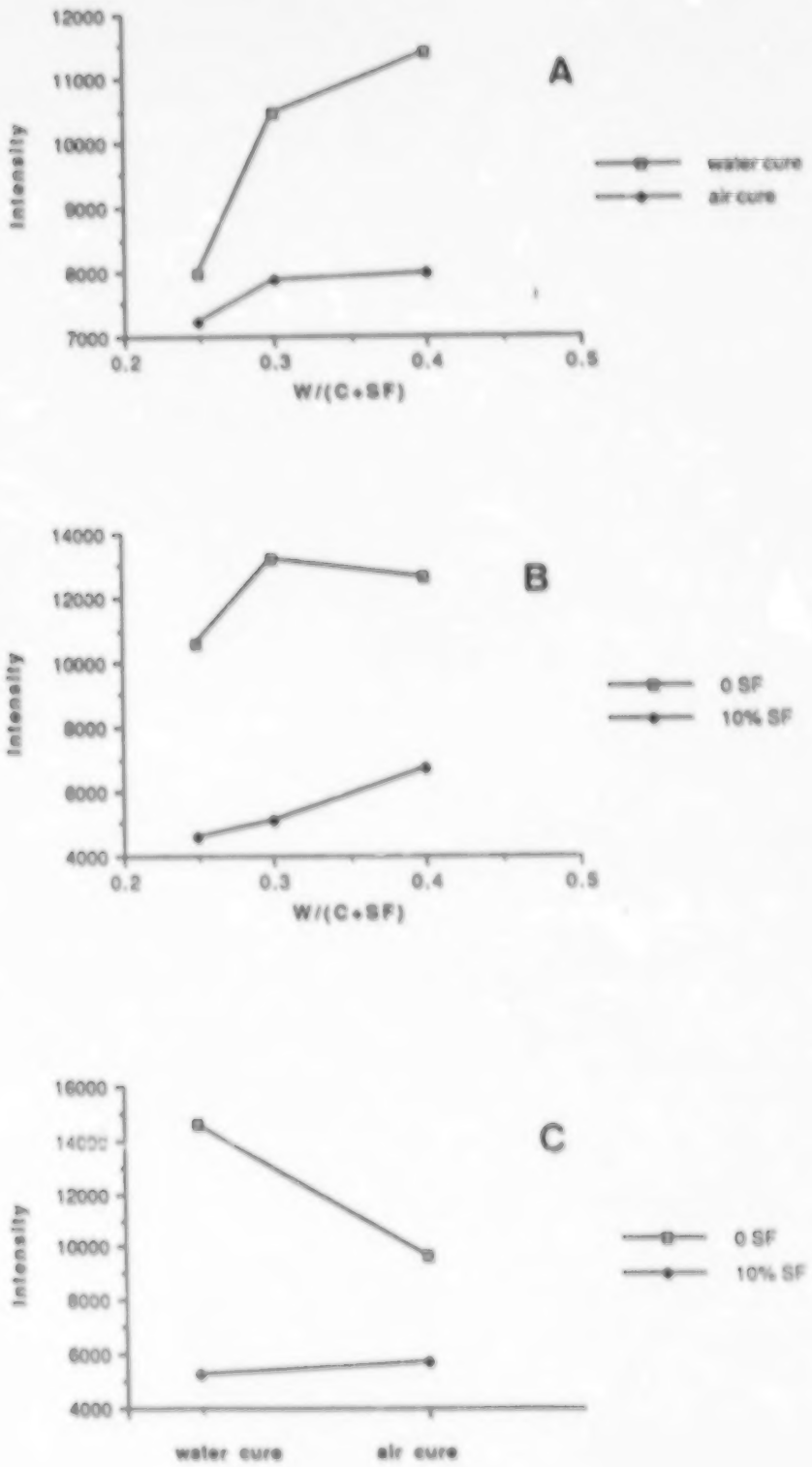

Fig. 107 Analysis of influence of different factors upon CH generation

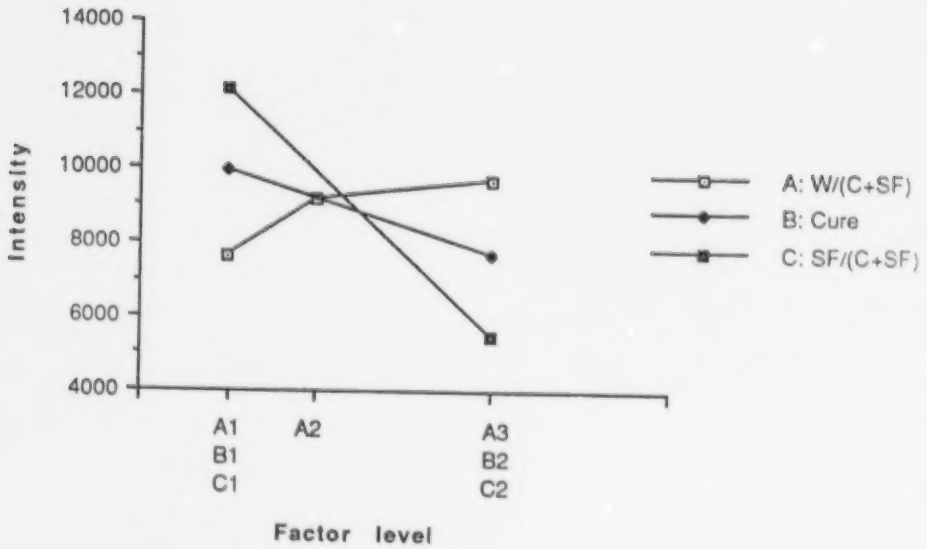

Fig. 108 Summarized plot of the three different factors

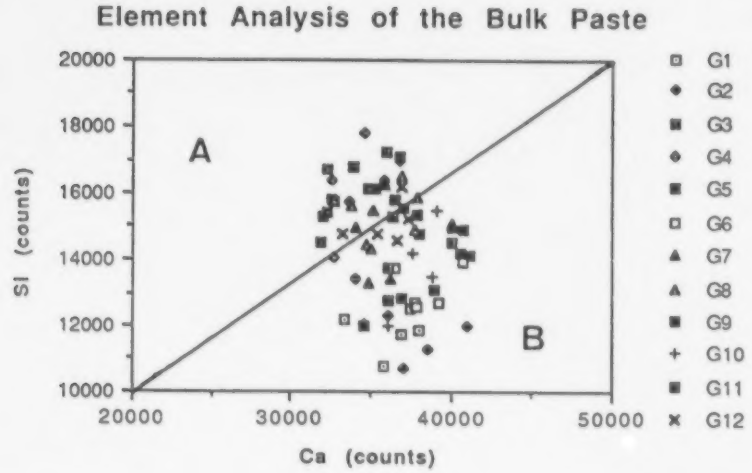

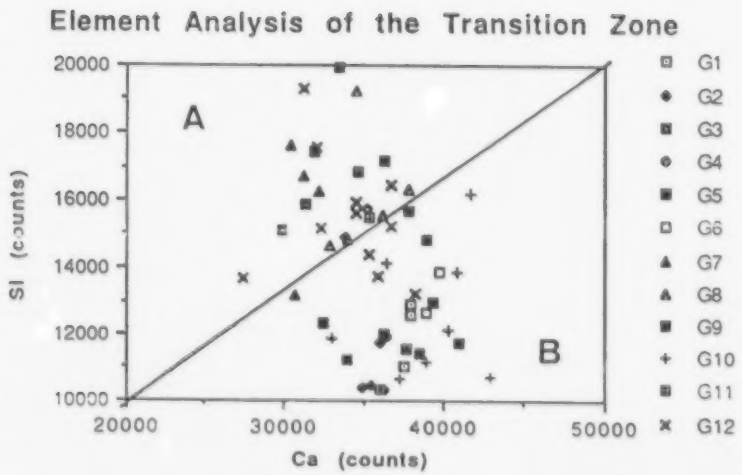

Fig. 110 Ca versus Si plots of C-S-H in the bulk paste and transition zone

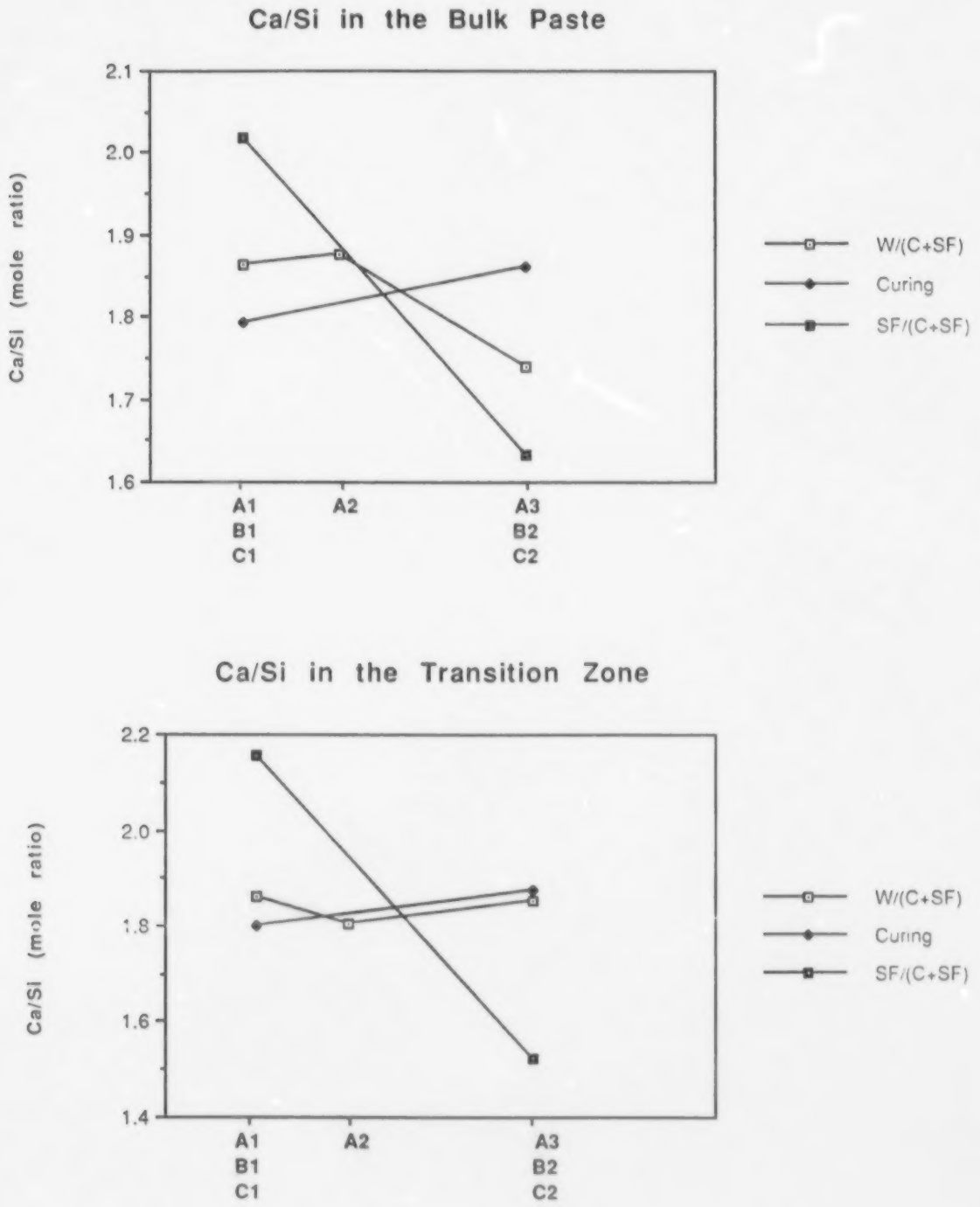

Fig. 111 Analysis of the effects of the three influencing factors

The Ca/Si ratio decreases in the paste region with increase in W/C+SF ratio from 0.25 to 0.40. A reverse trend is observed in the transition zone.

A combined effect of W/C+SF and SF/C+SF (SF replacement) is seen to exist (Fig. 112). For the control concretes, the Ca/Si ratio decreases as the W/C ratio increases, whereas it increases sharply from 0.25 to 0.30 for the silica fume concretes, then decreases slightly up to W/C+SF = 0.40.

The highest Ca/Si ratio (2.8) was recorded for G10, W/C = 0.40, air cured concrete, adn the lowest (1.13) for G12, W/C+SF = 0.40, also air cured concrete.

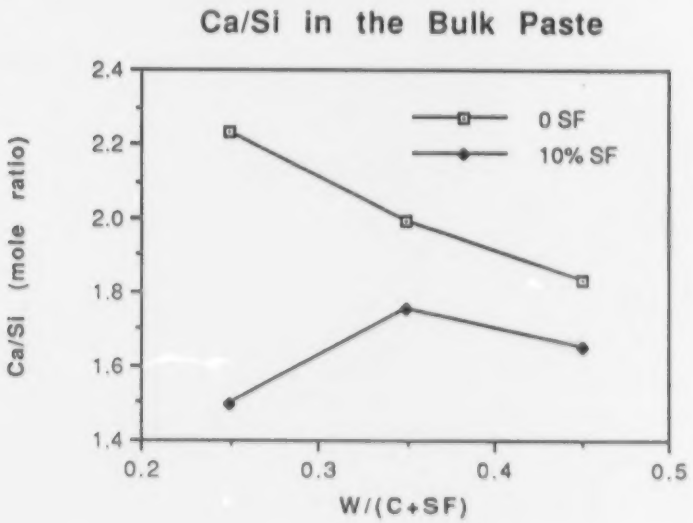

Fig. 112 Analysis of the two-factor interaction between W/C+SF and SF/C+SF

The histograms of Ca/Si in the paste and transition zone (Fig. 113) shows the following:

(i) Ca/Si ratio of C-S-H in the paste and transition zone of SF concretes is lower than that of control concretes. This confirms the F-test results (Fig. 111).

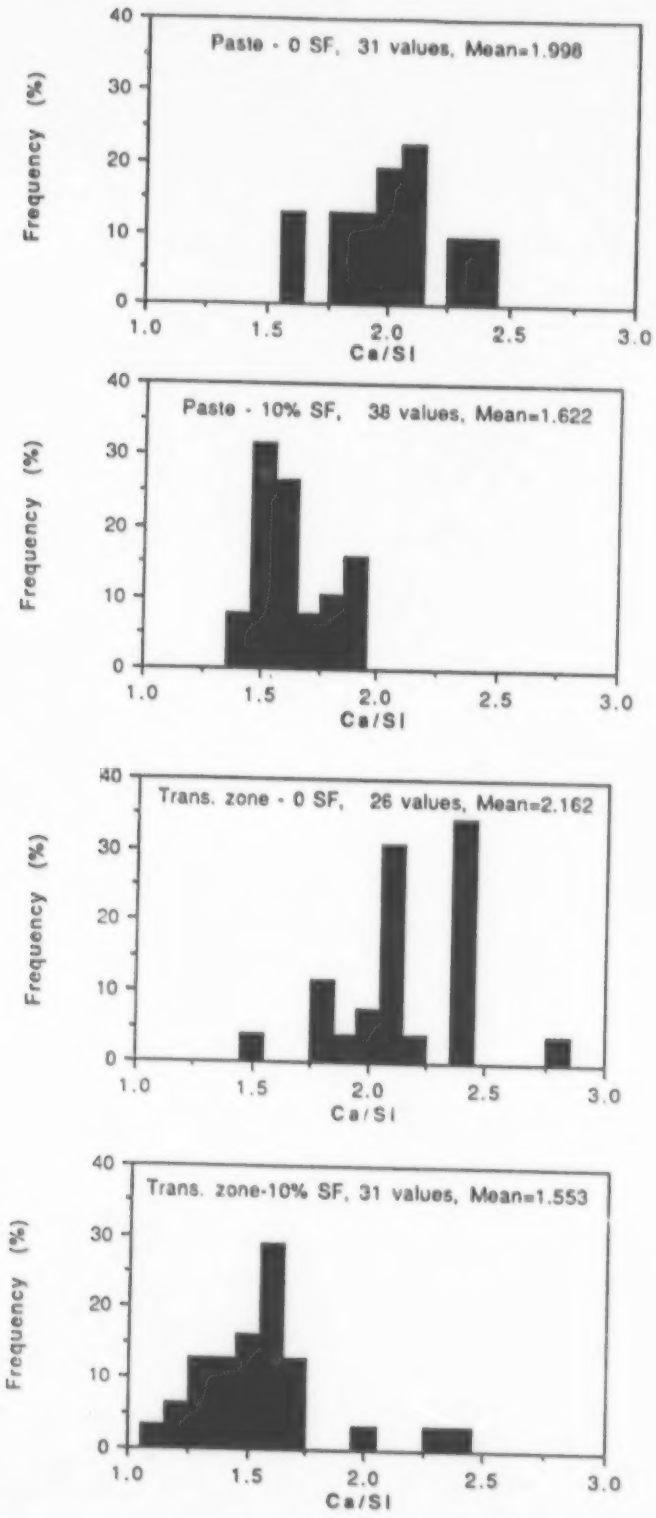

Fig. 113 Histograms of Ca/Si in paste and transition zone

(ii) The bimodal distribution in some of these histograms suggests the existance of two types of C-S-H.

The normalized frequency histogram is presented in Figure 114.

Fig. 114 Normalized frequency histogram